HHS Public Access

Author manuscript

Cell Rep. Author manuscript; available in PMC 2025 April 26.

Published in final edited form as:

Cell Rep. 2025 March 25; 44(3): 115366. doi:10.1016/j.celrep.2025.115366.

Distinct features of a peripheral T helper subset that drives the B cell response in dengue virus infection

Asgar Ansari[1], **Shilpa Sachan**[1], **Jatin Ahuja**[2], **Sureshkumar Venkadesan**[3], **Bhushan Nikam**[1], **Vinod Kumar**[2], **Shweta Jain**[2], **Bhanu Pratap Singh**[1], **Poonam Coshic**[4], **Kapil Sikka**[5], **Naveet Wig**[2], **Alessandro Sette**[6,7], **Daniela Weiskopf**[6,7], **Debasisa Mohanty**[3], **Manish Soneja**[2], **Nimesh Gupta**[1,8,*]

[1]Vaccine Immunology Laboratory, National Institute of Immunology, New Delhi 110067, India

[2]Department of Medicine, All India Institute of Medical Sciences, New Delhi 110029, India

[3]Bioinformatics Center, National Institute of Immunology, New Delhi 110067, India

[4]Department of Transfusion Medicine, AIIMS, New Delhi 110029, India

[5]Department of Otorhinolaryngology, Head and Neck Surgery, AIIMS, New Delhi 110029, India

[6]Center for Vaccine Innovation, La Jolla Institute for Immunology, La Jolla, CA 92037, USA

[7]Department of Medicine, Division of Infectious Diseases and Global Public Health, University of California, San Diego (UCSD), La Jolla, CA 92037, USA

[8]Lead contact

SUMMARY

Dengue-virus-induced humoral immunity can increase the risk of severe disease, but the factors influencing this response are poorly understood. Here, we investigate the contribution of $CD4^+$ T cells to B cell responses in human dengue infection. We identify a dominant peripheral $PD\text{-}1^+$ T cell subset that accumulates in severe patients and could induce B cell differentiation via interleukin-21 (IL-21)-related pathway. Single-cell analyses reveal heterogeneity within $PD\text{-}1^+$ cells, demonstrating the coexistence of subsets with “helper” ($IL\text{-}21^+$) or “cytotoxic”

*Correspondence: nimesh.gupta@nii.ac.in.

AUTHOR CONTRIBUTIONS

N.G. conceptualized and supervised the study. M.S. and N.W. enrolled and clinically assessed patients with dengue. K.S. enrolled and collected tissue samples. P.C. collected blood from healthy donors. J.A., V.K., S.J., B.P.S., A.A., and S.S. were responsible for sample collection. A.S. and D.W. gathered resources (DENV peptide pool). A.A., S.S., and B.N. conducted investigations. A.A., S.S., S.K., D.M., and N.G. conducted formal analysis. A.A. and N.G. wrote the manuscript. N.G. and A.S. acquired funding. All authors edited and reviewed the final manuscript.

DECLARATION OF INTERESTS

N.G. and A.A. are listed as inventors on patents submitted by the National Institute of Immunology and cover the use of the “T cell qualitative assay” for vaccine evaluation. N.G. has filed patent protection for the use of dengue virus Tfh epitopes identified in the Indian population. D.W. is a consultant for Moderna. La Jolla Institute for Immunology has filed for patent protection for various aspects of T cell epitopes and vaccine design work. A.S. is a consultant for GritstoneBio, FlowPharma, Moderna, AstraZeneca, Qiagen, Fortress, Gilead, Sanofi, Merck, RiverVest, MedaCorp, Turnstone, NAVaccine Institute, Emervax, GersonLehrman, and Guggenheim.

SUPPLEMENTAL INFORMATION

Supplemental information can be found online at https://doi.org/10.1016/j.celrep.2025.115366.

characteristics. The IL-21$^+$ subset displays a distinct clonotypic and transcriptomic signature compared to follicular helper T cells and persists as a memory in lymph nodes. Notably, we show that the IL-21$^+$ subset seems to majorly drive the extrafollicular B cell responses in dengue. Our study establishes the peripheral IL-21$^+$ subset as a potential determinant of the humoral response to dengue virus infection. These findings provide important insights into the T-cell-dependent regulation of humoral responses and can inform the design of effective dengue vaccines.

Graphical Abstract

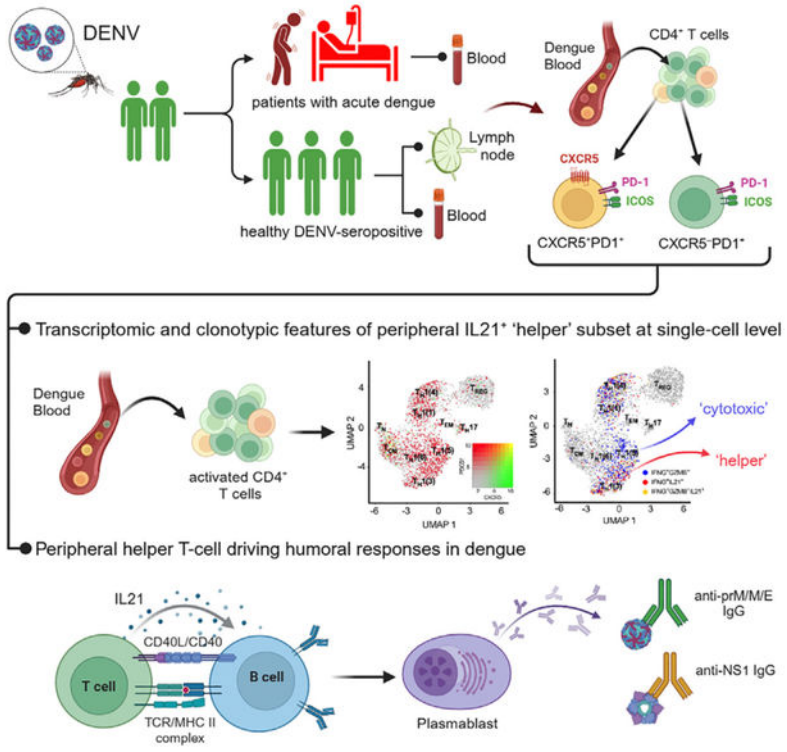

In brief

Ansari et al. identify a peripheral PD-1$^+$CD4$^+$ T cell subset in dengue that drives B cell differentiation via IL-21 axis. Single-cell analyses uncover distinct non-follicular “helper” and “cytotoxic” subsets in PD-1-expressing cells. This study provides important insights about T cell-B cell interactions, highlighting IL-21$^+$ helper subset as a driver of non-canonical humoral responses in dengue.

INTRODUCTION

Dengue is a mosquito-borne viral disease that causes ~400 million infections worldwide annually, approximately 100 million of which are clinically apparent.[1] Symptomatic dengue ranges from a self-limiting mild illness, dengue fever (DF), to life-threatening severe forms, dengue hemorrhagic fever (DHF) or dengue shock syndrome.[2] In particular,

individuals with secondary infections are at greater risk of severe disease. Although the underlying immunopathogenic mechanisms are not fully understood, cross-reactive and poorly neutralizing antibodies are believed to be significant contributors to severe disease.[3–10] Apparently, a lower concentration of subneutralizing and cross-reactive antibodies can mediate susceptibility to enhanced disease, which may occur a few months after the first infection.[11]

These studies highlight the fact that not only antibody durability but also inefficiency in generating optimal memory B cells might lead to poorly protective humoral immunity in patients with dengue. Dengue virus (DENV) memory B cells persist in circulation for several years but are dominated by cross-reactive antibodies with low or no neutralizing potency, in addition to rare populations of potent neutralizing antibodies.[12] This is particularly interesting in the context of vaccination, where despite its ability to induce a neutralizing antibody response, the tetravalent dengue vaccine was unable to confer sufficient protection against virus infection.[13] On the other hand, massive expansion of plasmablasts occurs in patients with acute dengue[14] and is correlated with severe outcomes.[15,16] Moreover, memory-derived plasmablasts that produce cross-reactive neutralizing antibodies and target conserved epitopes on DENV serotypes have also been reported in secondary dengue.[17,18] These studies indicate the possible implication of more than one mechanism in the generation of memory B cells and plasmablasts in dengue. However, considering the magnitude and durability of memory B cells in dengue, it is likely that the majority of B cell responses are the productive outcome of $CD4^+$ T cell and B cell collaboration.

Several studies have explored the role of $CD4^+$ T cells in dengue. Most of these studies elegantly described the antiviral and cytotoxic functions of $CD4^+$ T cells in dengue.[19,20] However, there is limited knowledge available on the type and function of $CD4^+$ T cells that drive humoral immunity to DENV infection. A specialized subset of $CD4^+$ T cells, follicular helper T (Tfh) cells, is known to drive protective B cell and antibody responses in germinal centers.[21,22] Indeed, the presence of circulating counterparts of Tfh cells has been shown in patients with dengue and is correlated with the plasmablast response.[23] Although plasmablast responses during the acute phase correlate well with the frequency of activated peripheral Tfh (pTfh) cells, it is unlikely that germinal center (GC)-Tfh cells alone contribute to the massive expansion of cross-reactive plasmablasts during acute DENV infection.[14,15,24,25] Indeed, a recent report suggested coordinated responses of Granzyme B^+ $CD4^+$ T cells and $Ki67^+$ plasmablasts.[26] Thus, considering the decisive role of the humoral response in dengue pathophysiology, understanding the mechanistic axis of $CD4^+$ T cell-B cell collaboration during humoral immunity development to dengue virus is critical.

In this study, we delineated the mechanism by which $CD4^+$ T cell subsets drive humoral responses to DENV. We utilized a longitudinal cohort of patients with acute dengue to investigate the traits and dynamics of $CD4^+$ T cell and antibody responses during primary and secondary dengue and in various outcomes of disease. We found that patients with secondary infections had early expansion of $CD4^+$ T cells and antibodies, and severe cases were predominantly in the extended phase of acute infection. We report the presence of a novel DENV-specific programmed cell death protein 1 (PD-1)-expressing peripheral $CD4^+$

T cell subset that accumulated more in dengue patients, with increased warning signs and disease severity. This peripheral $CD4^+$ subset showed a positive correlation with *in vivo* expansion of plasmablasts and with antibodies against non-structural protein NS1 and pre-membrane/membrane/envelope protein (prM/M/E), which was greater than that of DENV Tfh cells. It exhibited "B cell helper" properties and can promote plasmablast differentiation in *ex vivo* T-B cocultures, mainly through the interleukin-21 (IL-21) helper signaling axis. Using single-cell transcriptomic analyses, we further showed that this B cell helper subset may migrate to inflamed tissues and is a clonally distinct IL-21^+ subset in the pool of highly heterogeneous PD-1-expressing cells, along with another subset that harbors cytotoxic functions. Finally, we provide evidence of an extrafollicular B cell phenotype in patients, which strongly correlates with this peripheral "B cell helper" subset. Our findings provide insight into the existence of non-canonical pathways involved in the B cell response in dengue that might originate in lymphoid and non-lymphoid tissues with the help of the peripheral IL-21^+ T cell subset.

RESULTS

Phenotype of proliferating $CD4^+$ T cells in the blood of acute dengue and their dynamicity during the course of disease

To understand the phenotype and dynamics of the $CD4^+$ T cell response during dengue, a total of 170 adult patients with acute dengue were enrolled in a hospital-based cohort (Tables S1 and S2). Blood samples were collected during the acute phase (mean ± SD, 6.7 ± 3.2 days of illness) after hospitalization. Some of the patients ($n = 32$) were longitudinally followed post discharge during an extended convalescence phase (33.7 ± 12.9 days post symptom onset) (Figure 1A and Table S3). Dengue was confirmed by detecting DENV NS1 antigen or DENV-specific immunoglobulins, IgM and IgG, in the patient's plasma. Clinical and demographic data were collected from patient records during hospitalization (Tables S1 and S2). Patients with unconfirmed dengue or coinfections were excluded from the study. The majority of the patients (~2/3) in the cohort experienced secondary DENV infection (Figure 1B), as indicated by the IgM-to-IgG ratio. We then analyzed $CD4^+$ T cells in the $CD45RA^-$ compartment of peripheral blood mononuclear cells (PBMCs) from a subgroup of acute patients ($n = 21$). We detected a large number of recently proliferating cells expressing Ki67 (Figures 1C and S1A). The proliferating cells expressed several activation-associated markers, including ICOS, CD38, and HLA-DR (Figures 1D and S1B). The $Ki67^+$ proliferating cells showed elevated expression of CXCR3 but not CCR6, suggesting that they were skewed toward the T helper 1 (Th1) phenotype. Further analysis revealed the existence of CXCR5-expressing Tfh cells as a minor subset (7.5% ± 1.0%). To better understand the coexpression of these phenotypic markers, we performed non-linear dimensional reduction analysis using t-distributed stochastic neighbor embedding (t-SNE) on memory $CD4^+$ T cells from patients with increased proliferation ($n = 9$) (Figures 1E and S1C). A distinct cluster of activated cells was located at the bottom of the t-SNE plot and coexpressed ICOS, CD38, PD-1, and CXCR3 but not CCR6. CXCR5 exhibited minimal occupancy within this activated cluster. Additionally, the activated cluster had a region with variable Ki67 expression and a relatively small region expressing HLA-DR (Figure 1E). To define the activation phenotype, we used $ICOS^+Ki67^+$ double-positive cells,

which included recently proliferating and activated cells. Moreover, combinatorial analysis confirmed that all $ICOS^+Ki67^+$ cells were equally represented by $ICOS^+CD38^+$ cells but not by $HLA\text{-}DR^+CD38^+$ cells (Figures S1D and S1E). These $ICOS^+Ki67^+$ activated cells had greater expression of CD38, PD-1, and CXCR3 (Figure 1F) than did their resting memory counterparts ($ICOS^-Ki67^-$). Next, we measured the dynamics of $CD4^+$ T cell activation during the acute phase in patients with primary and secondary dengue. We found a significant increase in activated T cells in primary dengue after 7.4 ± 1.4 days of illness compared to 4.3 ± 0.9 days of illness (Figure 1G). We also observed a similar increase in the frequency of activated cells expressing PD-1 during the later phase of acute illness (Figure 1I). Although secondary-dengue patients exhibited a significant increase in T cell activation during the early phase, the magnitude of T cell activation remained unchanged in the later phase of acute illness (Figures 1G and 1I). We then followed a subgroup ($n = 24$) of patients post discharge during an extended convalescence phase to examine T cell dynamicity during recovery. A significant 4-fold (median: 12.1%–3.1%) decrease in the frequency of activated T cells was observed in convalescent dengue (Figure 1H), which was also reflected by the decrease in PD-1-expressing cells similar to those in healthy donors (Figure 1J and Table S4). The waning of T cell activation in convalescent dengue was consistent in both primary- and secondary-dengue patients (Figures 1G and 1I). Overall, acute dengue is associated with robust activation and expansion of $CD4^+$ T cells within 1 week after the patient has developed either primary or secondary disease. The expanded T cells in circulation are composed of PD-1-expressing activated cells that swiftly undergo a resolution phase in which these cells seem to have contracted their size or migrated to peripheral tissues.

Exorbitant accumulation of $CXCR5^-PD\text{-}1^+CD4^+$ T cells in patients with dengue with warning signs and severe dengue

We next determined the frequency of subsets co-occurring with pTfh cells that expressed PD-1 (Figure 2A). The frequency of pTfh cells ($CXCR5^+PD\text{-}1^+$) was significantly greater (healthy donor [HD] 1.4%, DENV 3.6%; Figure 2B) in patients with dengue. In addition, the peripheral $CXCR5^-PD\text{-}1^+$ subset was highly accumulated (HD 11.7%, DENV 24.7%; Figure 2B). Interestingly, $CXCR5^-PD\text{-}1^+$ cells were the predominant subset in the activated T cell pool (~75%, Figure S2A) and exhibited greater activation and expansion than did pTfh cells ($CXCR5^+PD\text{-}1^+$, 15.9%; $CXCR5^-PD\text{-}1^+$, 32.3%; Figure 2C). To determine the association of these two activated subsets with disease outcome, we classified patients with acute dengue into dengue fever without warning signs (DF without WS, $n = 37$), DF with WS ($n = 116$), and severe dengue (severe bleeding, leakage syndromes, and organ involvement, $n = 33$) according to World Health Organization guidelines[27] (Tables S1 and S2). Only one sampling was performed for all the patients during the acute phase, except for approximately 16 patients (out of 170) whose samples were taken twice during hospitalization. The disease outcomes of these patients were classified based on their clinical and physical examination at the time of sampling. Consistent with the findings of previous studies, severe dengue was more strongly associated with secondary infection than was DF without WS (~76% versus ~49%, Fisher's exact test, $p = 0.02$) (Figure 2D). The frequency of total pTfh and $CXCR5^-PD\text{-}1^+$ cells was greater in patients with WS than in patients without WS. However, a consistently greater magnitude of $CXCR5^-PD\text{-}1^+$ cells was retained in severe dengue, which was not the case for pTfh cells (Figures 2E–2G). Notably,

the magnitude of these subsets did not differ between primary and secondary dengue for any disease outcome (Figures S2B and S2C). Unlike pTfh cells, which exhibited no changes in disease outcome (Figures 2H and S2D), $CXCR5^{-}PD\text{-}1^{+}$ cells exhibited strikingly greater frequency of activation ($ICOS^{+}Ki67^{+}$) in DF with WS and severe dengue (Figure 2I). In addition, $CXCR5^{-}PD\text{-}1^{+}$ cells were slightly more activated in patients with secondary dengue with or without WS but remained at similar levels during severe outcomes (Figure S2E). Thus, $CXCR5^{-}PD\text{-}1^{+}$ cells with an activated phenotype were more strongly associated with WS and severe disease outcomes. To further confirm that the $CXCR5^{-}PD\text{-}1^{+}$ cells do not contain regulatory T (Treg) cells, we analyzed $CD25^{+}FOXP3^{+}$ cells in dengue (Figures S2F and S2G). $CXCR5^{-}PD\text{-}1^{+}$ cells with increased PD-1 expression were present mainly in the non-Treg compartment (Figure S2G). Collectively, these data provide evidence for the excessive expansion of the peripheral $CXCR5^{-}PD\text{-}1^{+}CD4^{+}$ T cell subset in patients with pathologically progressive dengue with warning signs and severity.

Single-cell RNA-sequencing and TCR-sequencing analyses of activated $CD4^{+}$ T cells from acute dengue

As we found the strong evidence of increased expansion of $CXCR5^{-}PD\text{-}1^{+}$ cells in peripheral blood of acute dengue, we next explored the cellular heterogeneity and transcriptomic landscape of the PD-1-expressing $CXCR5^{-}$ subset in acutely ill patients with dengue. We thus performed single-cell transcriptome analyses of the activated $CD4^{+}$ T cell population ($ICOS^{+}CD38^{+}$), which was enriched for the majority of proliferating cells (Figure 3A). After applying the quality-control parameters of the analysis pipeline, a total of 4,361 activated T cells (pooled from three patients) were recovered for analysis (Figures S3A and S3B). We integrated the datasets using the Seurat canonical correlation analysis (CCA)-based method[28] and performed graph-based clustering after regression of confounding factors such as the number of unique molecular identifiers, number of genes, and percentage of mitochondrial genes to create a uniform manifold approximation and projection (UMAP) plot (Figures 3B, S3C, and S3D). UMAP analysis revealed ten distinctly positioned clusters in the dengue-activated $CD4^{+}$ T cell population, reflecting their unique transcriptional signatures (Figures 3B–3E). Clusters 0–6 consisted of the majority of cells, accounting for 95% of the total cells (Figures 3C and S3E). Differential gene expression analysis revealed highly enriched transcripts in each cluster, as shown in Figures 3D and 3E and Table S5A. The hierarchical ranking of clusters based on enriched transcripts identified clusters 9, 8, and 7 as very distinct rare clusters (Figure 3D). Cluster 0 was enriched with Treg (T_{REG}) cell gene signatures (*IL2RA*, *FOXP3*, *RTKN2*, and *IKZF2*) (Figure 3E). Cluster 2 presented gene signatures of T central memory (T_{CM}) cells (*TCF7* and *CCR7*). This cluster was located nearest to cluster 8 and included naive T (T_N) cell-like gene signatures and uniquely expressed *FHIT* and *SNED1*. Cluster 7 had an enrichment of Th17 (T_H17) cells and expressed *CCR6*, *CTSH*, and *KLRB1*. Clusters 5 and 6 were highly enriched for the effector T_H1 cell gene signatures *LAG3*, *GZMA*, *GZMK*, and *PRF1*. Clusters 3, 1, and 4 expressed the T_H1 gene along with the transcripts associated with the cell-cycle genes *MKI67*, *PCNA*, *MCM7*, and *TOP2A*, which was also confirmed by cell-cycle phase analysis (Figures 3E and 3F). Cluster 9 expressed the T effector memory (T_{EM}) genes (*CCL4* and *CCL5*) and uniquely upregulated the expression of two long non-coding RNAs (lncRNAs), *FP671120.4* and *FP236383.3*.

Next, we identified clusters expressing *CXCR5*, *PDCD1*, and *CXCR3* transcripts (Figures 3G, 3H, and S3F). We detected the expression of *PDCD1* transcripts in all the clusters except for clusters 0 (T_{REG}) and 8 (T_N), which accounted for ~77% of the total cells. Cells coexpressing *CXCR5* or *CXCR5* and *PDCD1* (~15%) were mostly present in cluster 2 (T_{CM}). Moreover, highly upregulated expression of *CXCR3* was found in clusters $T_H1(5)$, $T_H1(6)$, $T_H1(3)$, $T_H1(1)$, and $T_H1(4)$. These observations were further supported by the expression of cell surface proteins in these clusters (Figure S3F, csp). Interestingly, single-cell trajectory analysis revealed that the PD-1-expressing T_{CM}, $T_H1(5)$, $T_H1(6)$, and $T_H1(3)$ clusters were closely related, with a trajectory starting from a less differentiated T_{CM} to $T_H1(6)$ and subsequently branching into two alternative clusters, $T_H1(1)$ and $T_H1(4)$ at the top and $T_H1(5)$ and $T_H1(3)$ at the bottom (Figure 3I). Cluster $T_H1(6)$ appeared to constitute an intermediate T_H1 effector population whose expression extended downward into the more differentiated T_H1 effector cluster $T_H1(5)$ and later into the cell-cycling cluster $T_H1(3)$. Furthermore, cluster 0 (T_{REG}) exhibited a trajectory directly related to the proliferative clusters $T_H1(1)$ and $T_H1(4)$.

We then performed single-cell T cell receptor sequencing (TCR-seq) analysis to inspect the clonal relationships and expansions within these clusters. We found one hyperexpanded clonotype *TRAV13–1.TRBV2* (945 clones) and four large clonotypes, *TRAV29.TRBV11–2* (58 clones), *TRAV12–1.TRBV12–4* (47 clones), *TRAV21.TRBV5–1* (46 clones), and *TRAV26–1.TRBV19* (44 clones) (Figure S3G and Table S5B). The majority of hyperexpanded and large/medium expanded clonotypes were present in clusters $T_H1(5)$, $T_H1(6)$, $T_H1(3)$, $T_H1(1)$, and $T_H1(4)$, resulting in an average of at least 1.5 cells per clonotype observed in these clusters. On the other hand, cluster 0 (T_{REG}) and cluster 2 (T_{CM}) cells exhibited mostly single/small expanded clonotypes (Figures 3J, 3K, and S3H). Clonotype overlap analysis revealed a significant distribution of TCR clonotypes between the proliferative clusters $T_H1(1)$ and $T_H1(4)$ and other major clusters, including cluster 0 (T_{REG}) (Figures 3L–3M). Notably, the PD-1-expressing clusters $T_H1(5)$, $T_H1(6)$, and $T_H1(3)$ cells exhibited significant overlap (Figure S3I) but to a lesser extent with the Tfh cell subset containing cluster 2 (T_{CM}).

Certainly, these data suggested considerable heterogeneity in activated $CXCR5^{-}PD\text{-}1^{+}$ T cells, which were mostly composed of proliferative and T_H1 effector/effector memory subsets with hyper- and large expandability and significant clonal overlap. Moreover, the $CXCR5^{-}PD\text{-}1^{+}$ T cells in dengue seem to originate from a repertoire distinct from that of the pTfh subset, as apparent by the marginal clonal overlap between PD-1-expressing clusters and the Tfh-containing cluster.

The $CXCR5^{-}PD\text{-}1^{+}$ subset showed enrichment in DENV-specific $CD4^{+}$ T cells and remained detectable in blood of dengue-recovered individuals

With the clear indication of clonal expansion of T cells from single-cell analysis, we sought to evaluate the DENV antigen-specific cells in dengue blood to better understand the dynamics and stability of the T cell subsets discussed above. We analyzed DENV-specific T cells in PBMCs from dengue-infected patients stimulated with the megapool of CD4 T cell reactive peptide ($DENV_{pep}$) derived from all four DENV (DENV1–DENV4)

serotypes[29] via an activation-induced marker (AIM) assay. AIM analysis of a subset of acute patients ($n = 44$) revealed an average of 0.78% of DENV-specific cells in the total pool of $CD45RA^{-}CD4^{+}$ T cells (Figures 4A and 4B). Antigen-independent stimulation with the mitogen concanavalin A (ConA) induced an average response of 2.59% of the cells (Figure 4C). The DENV-specific T cells showed a significant increase from an average of 4–7 days of acute illness. Only 0.28% of DENV-specific T cells remained detectable in convalescent dengue approximately 34 days after symptom onset (Figures 4D and 4E). We next determined the enrichment of antigen-specific T cells in the CXCR5- and PD-1-expressing subsets (Figure S4A). Interestingly, the PD-1-expressing $CXCR5^{+}$ and $CXCR5^{-}$ subsets were more enriched in antigen-specific cells than was their PD-1-negative counterparts. Strikingly, greater enrichment of antigen-specific T cells was found in the $CXCR5^{-}PD\text{-}1^{+}$ subset than in the pTfh subset ($CXCR5^{+}PD\text{-}1^{+}$ 1.35%, $CXCR5^{-}PD\text{-}1^{+}$ 2.88%; Figures S4A and S4B), which was not the case with ConA stimulation. Although both subsets exhibited similar dynamic patterns until the recovery phase, the expansion of DENV-specific T cells was more apparent in the $CXCR5^{-}PD\text{-}1^{+}$ subset (Figures 4F and 4G). The reduction in the activated phenotype ($ICOS^{+}PD\text{-}1^{+}$) from acute (71.0%) to convalescent (33.8%) dengue indicated a shift in antigen-specific T cells from an activated effector to a memory phenotype (Figures S4C and S4D), which was also reflected in the Th1-like ($CXCR3^{+}CCR6^{-}$) skewed phenotype (Figures S4E and S4F). We further examined individuals who recovered from dengue (~10 months after symptom onset, Table S3) to investigate whether antigen-specific $CD4^{+}$ T cells acquired memory. Stimulation with $DENV_{pep}$ resulted in approximately 0.17% antigen-specific circulating T cells (Figure 4H), which comprised a $CXCR5^{-}PD\text{-}1^{+}$ subset marked with a Th1 memory phenotype (Figures 4I–4K). To determine whether this memory subset also existed in the lymphoid organs, we examined the lymph node (LN) tissues of DENV-seropositive individuals from the dengue endemic region who were previously exposed to DENV. Although among the total Tfh subsets, $CXCR5^{+}PD\text{-}1^{+}$ and GC-Tfh cells ($CXCR5^{++}PD\text{-}1^{++}$) were highly enriched in secondary lymphoid organs (LNs), interestingly we found similar frequencies of the total $CXCR5^{-}PD\text{-}1^{+}$ subset in paired LN tissue and blood (Figures S4G and S4H). Antigen-specific stimulation with $DENV_{pep}$ detected DENV-specific $CXCR5^{+}PD\text{-}1^{+}$ and $CXCR5^{-}PD\text{-}1^{+}$ cells in the LN tissues of these virus-exposed individuals. However, the peripheral blood and LN tissue cells exhibited variable responses to antigen-specific stimulation (Figures S4I and S4J).

Taken together, these findings demonstrate the expansion of DENV-specific $CD4^{+}$ T cells in the blood of acute dengue, predominantly within the $CXCR5^{-}PD\text{-}1^{+}$ subset. Although the frequency of $CXCR5^{-}PD\text{-}1^{+}$ cells significantly declined during recovery, these cells acquired a memory-like phenotype that persisted long term both in blood and lymphoid tissues.

Activated $CXCR5^{-}PD\text{-}1^{+}CD4^{+}$ T cells are positively associated with expanded plasmablasts and antibody response in dengue

As the PD-1-expressing subset showed dominance and co-occurrence with the pTfh subset, we attempted to determine the associations of these subsets with the antibody response in patients with dengue infection. We thus measured anti-NS1 and anti-prM/M/E IgG in

acute and convalescent dengue plasma. As in T cells, in primary-dengue patients there was a gradual increase in anti-NS1 IgG, while an early and significantly greater response was detected in secondary-dengue patients at all time points (Figures 5A and S5A). Similar results were observed for the anti-prM/M/E IgG titers (Figure S5B). Similarly, both cross-sectional (Figure 5A) and longitudinal (Figure 5B) anti-NS1 IgG levels continued to increase during recovery, which was not the case for anti-prM/M/E IgG (Figures S5B and S5C), consistent with the longer availability of the NS1 antigen but not of virion particles during disease progression.[30] Notably, the antibody response to both antigens was significantly greater in the severe dengue group than in the DF with WS group (anti-NS1; $p = 0.04$; Figure 5C) (anti-prM/M/E; $p = 0.03$; Figure 5D). Unlike binding antibodies, the DENV-neutralizing potential ($Neut_{50}$ titers) was comparable between these two groups (Figure 5E). However, cross-sectional and longitudinal levels of DENV-neutralizing titers in acute and convalescent dengue showed a trend similar to that of anti-prM/M/E antibody titer, with an increased magnitude in secondary compared to primary dengue at all time points (Figures S5D and S5E). CXCL13 plays a critical role in T-B crosstalk and may indicate a productive GC response.[31] We found significant levels of CXCL13 in both primary- and secondary-dengue patients at early onset (2–5 days of illness) of acute disease (Figure S5F), suggestive of active GC activity in acute dengue. However, CXCL13 levels remained elevated in both primary and secondary dengue, with slightly lower levels observed in secondary dengue between 6 and 11 days of illness (Figure S5F). Subsequently, CXCL13 levels decreased to basal levels during the convalescence phase (Figures S5F and S5G). Thus, CXCL13 levels were found to follow a trend similar to that of $CD4^+$ T cell responses. As an output of T-B crosstalk, we next evaluated antibody-producing B cells, called plasmablasts, in acute disease. We found strong evidence of plasmablast differentiation in acute patients ($p < 0.0001$; Figures 5F and S5H). Most of these plasmablasts expressed Ki67, CD27, CD71, and CXCR3 but downregulated the expression of CD19 and CD20, indicating their effector phenotype (Figures 5G, 5H, and S5I). To establish the biological relevance of the expanded $CD4^+$ T cell subsets in relation to humoral responses, we performed correlation analyses. Unlike activated pTfh ($CXCR5^+PD\text{-}1^+$), which was positively associated only with plasmablasts, the expansion of activated $CXCR5^-PD\text{-}1^+$ T cells was strongly positively correlated with both antibodies (anti-NS1 and anti-prM/M/E IgG) and plasmablasts of the acute phase of dengue (Figure 5I). However, both of these subsets showed no correlation with the neutralizing antibodies (Figure 5I).

Taken together, these data provide an overall understanding of antibody and plasmablast responses during acute dengue. Certainly these responses were strongly associated with the $CXCR5^-PD\text{-}1^+$ subset, indicating the role of this subset in regulating humoral immunity in dengue.

Antigen-specific $CXCR5^-PD\text{-}1^+CD4^+$ T cells robustly secrete B cell helper cytokines and are capable of promoting B cell responses via the IL-21 signaling axis

The strong association of the $CXCR5^-PD\text{-}1^+$ subset with *in vivo* antibody and plasmablast response instigated a detailed investigation of its B cell help potential. We first examined the production of CD40L and interferon-γ (IFN-γ) in *ex-vivo*-stimulated PBMCs with

$DENV_{pep}$ for a short time (~6 h) via an intracellular cytokine staining (ICS) assay. $DENV_{pep}$ stimulation induced a significant increase in the number of CD40L- and IFN-γ-producing cells in memory T cells (Figure 6A). On average, 1.36% and 1.04% of the DENV-reactive IFN-γ^+ and $CD40L^+$ cells, respectively, were present in acute patients (Figure 6B). There was a significantly greater frequency of DENV-reactive T cells coexpressing IFN-γ and CD40L ($p = 0.0002$; Figure 6C). Moreover, most of these cytokine producers (CD40L, IFN-γ, and IL-10) were enriched in T cells expressing PD-1 and CXCR3, indicating the presence of functionally potent DENV-specific Th1 effector cells (Figure 6D). We next analyzed the cytokine-producing ability of the $CXCR5^+$ and $CXCR5^-$ subsets of PD-1-expressing T cells and found that the $CXCR5^-$ cells contained significantly more DENV-specific cytokine producers (Figures 6E and 6F). Even after TCR-independent stimulation, the $CXCR5^-$ subset expressed significantly more IFN-γ than did the $CXCR5^+$ subset, although the two subsets expressed CD40L at equal levels (Figure 6E). We further confirmed the cytokine secretory function of the sorted, purified $CXCR5^+$ and $CXCR5^-$ subsets, which was like the findings of the IFN-γ-ICS analysis (Figure S6A). Because the cytokine IL-21 is important for B cell differentiation and function, we also examined IL-21 secretion in these sort-purified subsets. ELISpot analysis revealed that the $CXCR5^-$ subset can produce and secrete significant amounts of IL-21 compared to the $CXCR5^+$ subset upon stimulation with both antigen-specific and mitogen conditions ($DENV_{pep}$ $CXCR5^+$: 73 spot-forming units [SFUs]/million; $DENV_{pep}$ $CXCR5^-$: 128 SFUs/million; Figure S6B). To determine whether the cytokine-producing $CXCR5^-$ subset can also engage B cells in productive crosstalk, we utilized our recently described autologous T-B coculture assay.[32] Here, the B cell helper activity of the $CXCR5^-$ subset was measured in autologous cocultures with sort-purified B cells in DENV-specific settings. Activated T cells from acute disease patients exhibited poor survival after long-term (up to 9 days) coculture (data not shown). Therefore, we used memory $CD4^+$ T cells from DENV-seropositive individuals with significant DENV-reactive IgG titers (Figure S6C). Naive T cells failed to elicit a B cell response due to insufficient peptide-reactive T cells (Figures 6G and 6H). On the other hand, upon $DENV_{pep}$ stimulation, both $CXCR5^+PD\text{-}1^+$ and $CXCR5^-PD\text{-}1^+$ cells strongly promoted plasmablast differentiation. Unlike in memory $CXCR5^+$ cells, in which both $PD\text{-}1^+/PD\text{-}1^-$ subsets elicited similar B cell responses, only $CXCR5^-PD\text{-}1^+$ cells produced significantly greater B cell outputs than did their $PD\text{-}1^-$ counterparts. Similarly, like pTfh cells, $CXCR5^-PD\text{-}1^+$ cells elicited detectable antibody responses in the coculture supernatant for the majority of the donors tested (5/8 donors; Figures S6D and S6E) for both the DENV NS1 and prM/M/E antigens. Notably, only memory B cells, not naive B cells, responded preferentially to the B cell help provided by $CXCR5^-PD\text{-}1^+$ and pTfh cells (Figures 6I and S6F). Tfh cells secrete IL-21, IL-10, and IL-4, which are major helper axes that promote plasmablast differentiation and class switching.[33,34] Thus, we further attempted to identify the dominant cytokine regulating the help axis of $CXCR5^-PD\text{-}1^+$ cells by blocking the activity of the cytokines IL-21, IL-10, and IL-4 in cocultures. With respect to $CXCR5^-PD\text{-}1^+$ T cell cocultures, we observed a strong reduction in plasmablast output in the IL-21-blocking condition (~60%, Figure 6J) and a moderate reduction in plasmablast output after blocking IL-10 (~25%), but not after inhibiting IL-4, which is a prominent Th2 cytokine. This finding was consistent with the help axis utilized by pTfh cells (Figure S6G).

Taken together, these data indicated that the DENV-specific T cells within the CXCR5^{-}PD-1^{+} subset were functionally effective at secreting effector cytokines, including those required for B cell help, and that the cytokine-producing cells were largely enriched in PD-1-expressing subsets. Moreover, the CXCR5^{-} PD-1^{+} subset is capable of productive collaboration with B cells in antigen-specific settings, which is mostly driven by the IL-21 signaling axis.

Distinct features of the B cell helper subset in the CXCR5^{-}PD-1^{+} population with tissue migration patterns and strong associations with extrafollicular B cells in dengue

A greater B cell helper activity and strong association with antibody responses prompted us to investigate the functional signatures of CXCR5^{-}PD-1^{+} T cell subsets with B cell helper traits. Using single-cell RNA-sequencing (RNA-seq) data, we closely examined the gene signatures of PD-1-expressing clusters $T_H1(5)$, $T_H1(6)$, and $T_H1(3)$. We found that cluster $T_H1(5)$ presented the highest expression of *PDCD1* together with other activating and coinhibitory genes (Figures 7A and S7A). In addition, cluster $T_H1(5)$ cells strongly enriched T_H1 effector cytokines, including *IFNG*, *GZMA*, *PRF1*, and *GZMB* (Figures 7A and 7B; Table S6A). Most of these cytokines confer cytotoxic effects and are upregulated by type 1 interferon signaling. Gene set enrichment analysis (GSEA) also revealed strong cytotoxic CD4^{+} T cell and interferon response signatures in these clusters. This cluster also showed the highest positive enrichment of both these signatures (Figures S7B and S7C) expressing the important T_H1 transcriptional regulators *TBX21*, *STAT4*, and *RUNX3* (Figure 7A). Notably, cells in clusters $T_H1(5)$, $T_H1(6)$, and $T_H1(3)$ exhibited strong tissue migration markers and expressed various chemokine receptors and integrins (*CCR2*, *CCR5*, *CXCR3*, *CX3CR1*, and *S1PR1*). The clusters also showed the expression of adhesion molecules important for differentiation and function, *SH2D1A*, *SLAMF1*, and *SLAMF6*. In addition, cluster 2 (T_{CM}) cells strongly expressed the Tfh-associated transcriptional regulators *TCF7*, *LEF1*, *TOX2*, *BCL6*, and *ID2* and the migration genes *CCR7*, *SELL*, *S1PR1*, and *CXCR5* (Figures 7A and S7A; Table S6A). Certainly, the data further confirmed that cluster $T_H1(5)$ was highly T_H1 polarized with cytotoxic CD4 signatures, while cluster 2 (T_{CM}) had a central memory and Tfh-related gene signature.

Importantly, the proliferative PD-1-expressing clusters, especially cluster $T_H1(3)$, presented the highest expression of *IFNG*, *CD40LG*, and *IL21* (Figure 7B). As demonstrated above and as IL-21 signaling is the major B cell help axis utilized by the PD-1-expressing subset, we identified *IFNG*$^{+}$ cells expressing the *GZMB* and *IL21* transcripts to distinguish between the Th1 cytotoxic and helper subsets, respectively (Figure 7C). Interestingly, we found that the *GZMB*$^{+}$ cells, which were mainly enriched in clusters $T_H1(5)$ and $T_H1(6)$, had no significant coexpression with *IL21*$^{+}$ cells, but the *IL21*$^{+}$ cells, which were enriched in proliferative clusters $T_H1(3)$, $T_H1(1)$, and $T_H1(4)$, showed some coexpression with *GZMB*$^{+}$ cells (Figure S7D). Polyclonal activation with the SEB antigen also confirmed the presence of two cell groups, one that expressed the cytokine IL-21 and one that expressed GZMB, among the memory CXCR5^{-}PD-1^{+} T cells (Figure S7E). We thus performed differential gene expression analysis between PD-1-expressing *IL21*$^{+}$ and *GZMB*$^{+}$ cells after excluding *GZMB*$^{+}$*IL21*$^{+}$ cells (Figure 7D and Table S6B). Among the cytotoxic *GZMB*$^{+}$ cells, those with genes related to cytotoxic function, *GZMA*, *GZMH*, *NKG7*, *PRF1*, and

GNLY, exhibited greater terminal differentiation. Strikingly, these cells presented increased expression of the *HOPX* transcription factor, which is induced by T-bet upon repeated antigenic stimulation and is enriched in terminally differentiated effector Th1 cells.[35] In addition, these cells upregulated *CD44* transcripts, which may promote their survival as Th1 effector memories.[36] In addition, helper *IL21*$^+$ cells appeared to be more proliferative than *GZMB*$^+$ cells because they expressed the key cell-cycle regulators *CDK6* and *CCND2* and had higher transcript levels of the glycolytic pathway, *PFKL* and *PKM*. *IL21*$^+$ cells expressed the mitochondrial chaperonins *HSPD1* and *HSPE1* and the antioxidant genes *MT1G*, *SOD1*, and *PRDX1*, which can support metabolic adaptations and protection from oxidative stress. Interestingly, these *IL21*$^+$ cells strongly expressed the *TOX2* transcription factor, which is expressed mainly by T_{CM} cells and might be essential for the maintenance of these helper cells in the central memory compartment. Importantly, *LGMN*, a key asparaginyl endopeptidase expressed in lysosomes, is highly expressed in *IL21*$^+$ helper cells. This enzyme has broad targets of substrates, including cathepsins and a1-thymosin, and can intrinsically promote Th1 activity in these helper cells.[37] Notably, compared with the double-negative or double-positive cells, the *IL21*$^+$ and *GZMB*$^+$ cells exhibited distinct gene landscapes (Figure 7E). However, the two cell groups, *IL21*$^+$ and *GZMB*$^+$ cells, expressed comparable levels of *PDCD1*, *MKI67*, *CCR2*, and *CCR5* (Figure 7F), suggesting that both contained CXCR5$^-$PD-1$^+$ proliferative cells and had similar tissue migration patterns. We further examined the clonotype diversity and found that only 13 TCR clonotypes were shared between the two cell groups, with 13/63 having *IL21*$^+$ and 13/136 having *GZMB*$^+$ cells (Figure 7G). TCR overlap was observed only in the highly expandable clones. These data indicate the existence of a pre-determined repertoire of multifunctional precursors that acquire either helper or cytotoxic features.

Circulating CXCR5$^-$PD-1$^+$ T cells showed strong signs of tissue migration, indicating active inflammation in peripheral tissues.[38] This was evident from the cytokine analysis data (Figure S7F), which showed the expression of the CXCR3 chemokine receptor ligands CXCL9 (MIG) and CXCL10 (IP-10), type 1 IFN, IFN-α2, and various proinflammatory cytokines—LIF, IL-1Rα, IL-1α, IL-2Rα, and IFN-γ. We thus hypothesized that these tissue-migrating T cells would interact with B cells at extrafollicular sites, including peripheral tissues, and elicit B cell responses. Therefore, we analyzed the extrafollicular B cells of patients with acute dengue and found that they had higher expression of CD11c but lower expression of CD21.[39] CD21$^-$CD11c$^+$ B cells in the blood of acute patients consisted mainly of IgD$^-$CD27$^-$ (double-negative [DN]) and IgD$^+$CD27$^-$ (naive) B cells, followed by IgD$^+$CD27$^-$ (switched memory) B cells (Figure S7G). However, extrafollicular B cells were more enriched among DN cells than among naive B cells (Figure 7H). The CD21$^-$CD11c$^+$ DN B cells presented increased CD19 expression but reduced CXCR5 expression, possibly because of their ability to migrate away from B cell follicles (Figure 7I). Remarkably, these extrafollicular (CD21$^-$CD11c$^+$ DN) B cells showed a strong positive association with activated CXCR5$^-$PD-1$^+$ T cells but not with CXCR5$^+$PD-1$^+$ (pTfh) cells (Figure 7J), suggesting their coordinated expansion and differentiation in acute dengue.

Collectively, our single-cell analysis clearly established substantial heterogeneity in CXCR5$^-$PD-1$^+$ T cells, which primarily consisted of specialized subsets with cytotoxic or helper functions. Notably, these data are the first evidence for the presence of extrafollicular

B cells in dengue, which seem to be induced by accumulating peripheral B cell helper T cell subset.

DISCUSSION

Severe dengue is often associated with secondary infections marked by rapidly expanding T and B cells and exaggerated humoral responses leading to immunopathology.[15,18,40,41] This study determines the contribution of $CD4^+$ T cell subsets to DENV-specific humoral responses and revealed the sizable accumulation of $CXCR5^-PD\text{-}1^+CD4^+$ T cells in patients with dengue with warning signs and severity. These cells are potent B cell helpers, driving plasmablast differentiation and antibody production primarily through the IL-21 help axis. They produced higher levels of CD40L, IFN-γ, and IL-10 than did the pTfh ($CXCR5^+PD\text{-}1^+$) cells. Most of these effector T cells accumulate during the first week of acute disease and subsequently wane during recovery. However, these cells with a Th1-type phenotype persisted in patients who recovered from dengue for a long period of time.

Consistent with previous findings, we observed that antibodies against the structural proteins prM/E and non-structural protein NS1 are associated with severe outcomes.[42] Anti-NS1 antibodies can mediate immunopathology by targeting complement components, platelets, and endothelial cells,[43–45] and anti-prM/E antibodies can promote disease via antibody-dependent enhancement (ADE) of infection.[46] In fact, anti-prM/M/E antibodies are highly cross-reactive and produced by expanding plasmablasts from cross-reactive memory B cells in secondary dengue.[14,18,47] Tfh cells seem not the only driver of these humoral responses in dengue, as their blood frequency or activation status remains unaltered in different disease outcomes despite progressive immune activation and severity. In line with our findings in an adult cohort, a study of Thai children also revealed no significant differences in pTfh frequency in DF and DHF patients.[23] However, the role of GC-Tfh cells in promoting neutralizing antibodies in dengue cannot be excluded, as we detected significant blood levels of CXCL13 as a surrogate of GC activity. A rare frequency of GC-Tfh cells efficiently migrate from lymphoid organs to the circulation as pTfh cells,[48] which can reflect a corresponding increase of pTfh cells in circulation. Certainly, in-depth studies are warranted to examine Tfh cells and GC activity in dengue. Indeed, in addition to pTfh cells, the $CXCR5^-PD\text{-}1^+$ subset also exhibited a positive association with *in vivo* plasmablast expansion and promoted plasmablast differentiation from memory B cells. These findings clearly suggested that B cell responses in dengue could be elicited in extrafollicular niches in addition to Tfh-dependent responses in B cell follicles. The predominance of the Tfh-independent B cell response was further supported by our finding that early generation of DENV-reactive antibodies in secondary dengue was sustained and positively associated with $CXCR5^-PD\text{-}1^+$ T cells but not with pTfh cells. In addition, the expanding plasmablasts in acute dengue expressed CXCR3 and CD71, which was also observed in COVID-19 and other acute viral diseases,[49,50] indicating that plasmablast differentiation occurs under the influence of IFN-γ, a cytokine extensively secreted by $CXCR5^-$ $PD\text{-}1^+$ T cells.

Remarkably, $CXCR5^-PD\text{-}1^+$ T cells constituted ~75% of the total activated $CD4^+$ T cells during acute dengue. Single-cell analyses revealed that these cells in acute disease are highly proliferative and mostly acquire the Th1 transcriptional program.[51,52] Certainly,

CXCR5^{-}PD-1^{+} Th1 cells constitutes a large population of effector cells in dengue, as indicated by their hyper- and large-expandability clonotypes. Interestingly, CXCR5^{-}PD-1^{+} cells were identified as a transcriptionally and clonally distinct subset of cells in dengue compared with Tfh cells, which mostly reflects the transcriptional signatures of central memory T cells.[53] Lymphoid tissue Tfh cells have been shown to exit the circulation via efferent lymphatics.[48] Similarly, in HIV infection, CXCR5^{-}PD-1^{+} T cells and Tfh cells in lymphoid tissue showed clonal similarities with their peripheral counterparts in blood.[54] These findings clearly suggest that the blood clonotypes may not be entirely distinct from those in lymphoid tissues. Considering the extensive transcriptional and clonal differences, it is likely that the CXCR5^{-}PD-1^{+} subset in dengue originates in lymphoid tissues from unique precursors, following differentiation pathways divergent from those of Tfh cells. Similarly, our results demonstrate that the Treg clonotypes in dengue are substantially more diverse than the pTfh or CXCR5^{-}PD-1^{+} subsets.

Surprisingly, single-cell analyses revealed substantial heterogeneity in the CXCR5^{-}PD-1^{+} subset, with enrichment of cytotoxic (*GZMA*, *GZMB*, and *PRF1*) and helper signatures (*IL21*, *SLAMF6*, and *MAF*). These data indicated that the CXCR5^{-}PD-1^{+} cell population included a subset with helper functions mostly enriched in IL-21-expressing cells, in addition to the subset harboring cytotoxic functions. A smaller fraction of cells coexpressing *IL21* and *GZMB* was also present in the proliferating CXCR5^{-}PD-1^{+} T cells that share a clonal lineage. However, these cells may represent intermediately differentiated cells that can further exhibit a terminally differentiated effector-memory-like phenotype. Indeed, PD-1-expressing cells in dengue include two distinct subsets that not only are distinct in their function but also have different developmental fates.

A phenotypically similar CXCR5^{-}PD-1^{+} subset called peripheral helper T (Tph) cells was identified in rheumatoid arthritis and systemic lupus erythematosus patients.[55–57] These cells exhibited activation and migration signatures consistent with our findings on the dengue cell subset. Additionally, in acute COVID-19 patients, Tph cells positively correlated with CXCR3-expressing plasmablasts *in vivo*, suggesting their role in regulating antibody responses via the IFN-γ axis.[50] These recently emerging studies revealed that acute or chronic diseases with highly inflammatory conditions can alter the functions of non-follicular (CXCR5^{-}) CD4^{+} T cells, where these T cells can acquire “B cell helper” functions in addition to their antiviral and cytotoxic functions. Our study revealed the existence of a distinct IL-21^{+} subset in the pool of PD-1-expressing cells that help B cells. It will be worthwhile to explore the role of the type 1 IFN pathway in promoting the differentiation of this subset.[58,59]

A strong expansion of plasmablasts in acute viral infections is associated with extrafollicular B cell responses.[39] Extrafollicular B cell responses appear early and precede GC reaction to promote antibody responses.[60] Extrafollicular B cells phenotypically belong to the DN (IgD^{-}CD27^{-}) subset with higher CD11c and CD19 but lower CD21 and CXCR5 expression.[39,61] Consistently, we found phenotypically similar extrafollicular B cells in acute dengue, which strongly associated with CXCR5^{-}PD-1^{+} T cells but not with Tfh cells. These results firmly suggest that the helper CXCR5^{-}PD-1^{+} T cell subset may drive plasmablast differentiation from extrafollicular B cells and can be associated with the

early production of large quantities of antibodies. Early antibody responses are highly evident in secondary dengue, where DENV serotype cross-reactive antibodies may lead to enhanced infection or targeting self-antigens (an autoimmune-like condition), causing aberrant activation and damage to platelets and endothelial cells.[45,62] Moreover, early and exaggerated plasmablast responses in extrafollicular compartments may negatively impact *de novo* GC development at later stages by producing a large quantity of tumor necrosis factor α.[63] This may limit the generation of serotype-specific neutralizing antibodies essential for controlling viral infection. Thus, $CXCR5^{-}PD\text{-}1^{+}$ T cell responses may provide a crucial link to the pathological generation of heightened antibody responses in severe dengue. Indeed, unlike blood, the limited presence of this memory subset in the lymphoid tissue of DENV seropositive individuals hints at the possibility of rapid expansion at the time of secondary infection. Interestingly, T cells induced in response to DENV infection express cutaneous lymphocyte-associated antigen (CLA), a skin-homing marker, and can migrate to the skin to exert their function.[64] In addition to CLA, we also found several migration-associated genes[65,66] on both helper and antiviral PD-1-expressing T cells that can promote their homing to extralymphoid inflamed tissues. It is possible that this peripheral helper subset contributes to robust plasmablasts and antibody responses in skin or inflamed tissues by helping B cells localize to these non-lymphoid sites. Future studies in the peripheral tissues of DENV-infected individuals probing the existence of such a T-B axis may provide further insight into our findings on the T cell determinants of humoral immunity in dengue.

In conclusion, our data essentially unveil the important immune axis of human response to dengue virus. We revealed the existence of a non-follicular B cell helper subset in dengue that is aberrantly accumulates in severe patients. This non-follicular helper subset shows clonotype and transcriptomic features distinct from those of pTfh cells and can be distinguished from the cytotoxic subset that coexists in the heterogeneous pool of PD-1-expressing $CD4^{+}$ T cells. Importantly, for the first time, these findings provide insight into the existence of extrafollicular B cell responses as an anomalous process of humoral responses in dengue, which seems to be driven by this non-follicular helper subset. Our study established $IL\text{-}21^{+}$ peripheral T cells as potential T cell determinants of the humoral response in dengue, which has implications for understanding disease biology and developing effective dengue vaccines.

Limitations of the study

This study is limited by a modest sample size and lack of simultaneous analyses of multiple cellular and serological analyses in all the subjects. Another limitation is the lack of direct evidence of $IL\text{-}21^{+}$ T cell interactions with extrafollicular B cells in DENV-infected tissues of patients. While increased CXCL13 levels are suggestive of productive GC reactions, our study does not provide in-depth analyses of dengue Tfh cells, particularly GC-Tfh cells in lymphoid tissues of patients with acute dengue. Moreover, the study shows neutralizing potential of antibodies against DENV-2 but lacks investigation on cross-reactivity to other serotypes and their potential role in disease-enhancing mechanisms such as ADE. Moreover, the peptide pool used to assess the antigen-specific $CD4^{+}$ T cells may not cover all epitopes in the viral genome. However, it includes most of the immunodominant epitopes, enabling

the detection of virus-specific $CD4^+$ T cells in the limited patient blood samples available. Certainly, future anti-gen-specific investigation of a larger prospective cohort will provide deeper insights into the T cell determinants of effective and durable humoral immunity to DENV.

RESOURCE AVAILABILITY

Lead contact—Further information and requests for resources and reagents should be directed to and will be fulfilled by the lead contact, Nimesh Gupta (nimesh.gupta@nii.ac.in).

Materials availability—This study did not generate new unique reagents.

Data and code availability—The published article includes all the datasets generated during this study. The scripts are available on Zenodo: https://doi.org/10.5281/zenodo.14632965. The sequencing data for this study have been deposited at the Gene Expression Omnibus and are publicly available as of the date of publication. Accession numbers are listed in the key resources table. Any additional information required to reanalyze the data reported in this paper is available from the lead contact upon request.

STAR★METHODS

Detailed methods are provided in the online version of this paper and include the following:

EXPERIMENTAL MODEL AND SUBJECT DETAILS

Ethics approval statement—This study was approved by the Institutional Ethical Review Boards of the National Institute of Immunology (NII) and All India Institute of Medical Sciences (AIIMS), New Delhi, India. Informed consent was obtained from all enrolled patients and healthy donors.

Dengue patients and samples—A prospective cohort of 170 adult patients with acute dengue hospitalized in the emergency and admission wards of AIIMS Hospital, New Delhi, between September and November 2017, 2018, and 2019 was enrolled in the study. The median age of the participants was 27 (IQR, 20–36) years, and 107 were male (63%). Blood samples were collected from patients with acute dengue during their hospitalization, with a median of 6 (IQR, 5–8) days of illness, and some of them ($n = 32$) were longitudinally followed postdischarge during the convalescence period, with a median of 34 (IQR, 24–42) days after the onset of symptoms. A small group of 7 patients was also longitudinally followed long-term, approximately 10 months after the onset of symptoms (Table S3). In all patients, acute DENV infection was confirmed by detection of the DENV NS1 antigen and/or by serological evidence, DENV-specific immunoglobulins, IgM and IgG. Clinical, demographic, biochemical, and comorbidity data are provided in Tables S1 and S2. Patients with unconfirmed dengue or other infections (e.g., malaria) were excluded from the study. According to WHO guidelines, acute dengue samples were categorized as dengue ± warning signs (WS) or severe dengue.[27]

Healthy donors—Peripheral blood buffy coats from healthy adult donors were collected from the AIIMS Hospital Blood Bank, New Delhi, India, between March 2017 and January

2020. Almost all the healthy donors were adult males (99%), with a median age of 30 (IQR, 26–36) years (Tables S1 and S4). Blood donor volunteers were free of any flu-like symptoms and had negative reports for infectious markers, HBV, HCV, HIV, and syphilis according to blood bank analyses.

LN tissue donors—Paired blood and lymphoid tissues (LNs and adenoids) were obtained from patients who underwent ENT-related surgical excision for biopsy analysis of malignant tumors/metastases. DENV virus exposure in these individuals was confirmed by anti-DENV IgG ELISA (Table S1).

METHOD DETAILS

PBMC and plasma processing—All the peripheral blood samples were processed within 4 h of collection to isolate peripheral blood mononuclear cells (PBMCs) and plasma. Whole-blood samples were collected in 10 mL K2 EDTA vacutainers for all dengue participants or in 350 mL CPD blood bags for all healthy blood donors. Whole blood was then centrifuged at 2000 rpm for 10 min to separate the plasma and cellular fractions. Then, 1–2 mL of plasma from the top was carefully removed from the remaining cell fractions and stored in aliquots at −80°C. PBMCs were separated by Ficoll gradient centrifugation using Ficoll-Paque PLUS (GE Healthcare Life Sciences), cryopreserved in several aliquots of heat-inactivated fetal bovine serum (FBS; Gibco) supplemented with 10% (v/v) DMSO (Thermo Fisher) and stored in liquid nitrogen until further analysis.

Dengue diagnosis and classification—Acute dengue infection was confirmed by detection of the DENV NS1 antigen or DENV-specific antibodies and IgM and IgG in the plasma samples. Table S2 depicts the timing of all these tests. The DENV NS1 antigen was detected and quantified by dengue NS1 sandwich ELISA (J. Mitra & Co. Pvt. Ltd., India). DENV-specific IgM and IgG antibodies were quantified by Panbio Dengue IgM (01PE20) and IgG (01PE10) capture ELISA kits (Abott). Samples were considered positive or negative according to the manufacturer's instructions according to the cutoff units. Equivocal or negative results were repeated when possible with consecutive sampling during hospitalization. Primary and secondary-dengue patients were classified as primary if the IgM/IgG OD ratio was > 1.2 (at a dilution of 1/100) or secondary if the OD ratio was ≤ 1.2 based on WHO guidelines. Healthy donor (HD) blood bank volunteers who were negative according to Panbio dengue IgG (01PE10) capture ELISA were selected as the HD control group. A highly sensitive Abcam human anti-DENV IgG ELISA kit (ab108728) was used to determine DENV seropositivity in HD volunteers.

DENV peptide pool—In all the autologous experiments, a DENV peptide pool (megapool) consisting of 180 different MHC class II binding peptides was used to stimulate antigen-specific $CD4^+$ T cells. This megapool of CD4 T cell reactive peptides was specifically designed to cover all four DENV (DENV1–4) serotypes that bind to a wide range of HLA types and was previously validated by intracellular cytokine staining assays.[29]

Flow cytometry and cell sorting—For phenotyping and functional analysis, cryopreserved PBMCs were thawed and revived by washing them with 10 mL of prewarmed

RPMI 1640 (Cytiva Life Sciences) and treated with DNase I (StemCell Technologies) at 100 μg/mL for 15 min at 37°C. The revived PBMCs used for downstream analysis were > 80% viable, as assessed by acridine orange (AO) and propidium iodide (PI) staining using an automatic LUNA-FL cell counter (LogoS Biosystems, Inc., USA). For direct *ex vivo* immuno-phenotyping of PBMCs, 1×10^6 PBMCs were surface stained with an antibody cocktail in FACS buffer (PBS with 2% FBS) for 1 h at 4°C in the dark. Following surface staining, the cells were washed with FACS buffer, fixed and permeabilized for 30 min at 4°C in the dark using an eBioscience Foxp3/transcription factor buffer kit (Thermo Fisher Scientific). Following fixation/permeabilization, the cells were washed with 1x permeabilization buffer and stained with intracellular/intranuclear antibodies in permeabilization buffer for 1 h at 4°C in the dark. The cells were subsequently washed twice with 1x permeabilization buffer and resuspended in 200 μL of FACS buffer. All the samples were acquired on a BD LSR Fortessa flow cytometer (BD Biosciences). All flow cytometry data were analyzed with FlowJo software v10.3.0. A list of the antibodies used for immunophenotyping of T and B cells is provided in Table S7A.

For the ELISPOT/FluoroSpot assays, PBMCs were surface stained with the anti-human antibodies mentioned in Table S7B in FACS buffer for 1 h. Memory $CD45RO^+CXCR5^+$ or $CD45RO^+$ $CXCR5^-$ cells were sorted via FACS from live $CD14^-CD16^-CD20^-$ $CD4^+$ cells. A pool of $CD20^+$ B cells and $CD14^+$ and $CD16^+$ monocytes was sorted together to serve as antigen-presenting cells (APCs). For the autologous coculture assay, PBMCs were surface stained as described above with the antibody cocktail shown in Table S7B. First, monocytes and B cells were sorted from live PBMCs as $CD14^+CD20^-$ and $CD14^-CD20^+$, respectively. Naive and memory B cells were sorted from $CD20^+$ B cells as $CD20^+CD27^-$ and $CD20^+CD27^+$, respectively. Similarly, memory and naive $CD4^+$ T cells were sorted from live $CD14^-CD20^-$ PBMCs as $CD4^+CD45RO^+$ and $CD4^+CD45RO^-$, respectively. Among the $CD45RO^+CD4^+$ T cells, CD25-expressing Treg cells were excluded prior to the sorting of memory cell subsets. The four memory cell subsets were then sorted based on the expression of CXCR5 and PD-1 in $CD45RO^+CD25^-$ cells. All the cell types were collected in RPMI 1640 medium (Gibco) supplemented with 50% FBS during FACS sorting. FACS was performed on a BD FACSAria Fusion flow cytometer (BD Biosciences) at medium flow rates using a 70 μm nozzle. For the IL-21 and GZMB costaining experiments, the $CXCR5^-PD\text{-}1^+$ $CD4^+CD45RO^+$ T cell subset was subjected to FACS using the same strategy as mentioned above.

Activation-induced cell marker (AIM) assay—Antigen-specific $CD4^+$ T cell analysis was performed using the highly sensitive AIM assay established by Crotty's laboratory.[73] In this assay, cryopreserved PBMCs were thawed, revived as described previously and resuspended in AIM-V medium (Gibco) in the presence of DENV peptides ($DENV_{pep}$;1 μg/mL) in a 96-well U bottom plate (Thermo Scientific) at 1×10^6 PBMCs per well. The cells were incubated for 18–20 h in standard culture conditions in a 37°C humidified incubator with 5% CO_2. Stimulation of cells with an equimolar amount of DMSO (vehicle; Sigma–Aldrich) was used as a negative control, and stimulation with concanavalin A (2 μg/mL; Sigma–Aldrich) was included as a positive control. After incubation, the cells were surface stained with an antibody cocktail in FACS buffer for 1 h in the dark at 4°C. The cells were

then washed with FACS buffer and fixed with 1% (w/v) paraformaldehyde (freshly prepared in 1x PBS; Sigma–Aldrich) for 30 min at 4°C in the dark. After fixation, the cells were washed twice with FACS buffer and resuspended in 200 μL of FACS buffer. The details of the antibodies used in the AIM assay are listed in Table S7C.

Intracellular cytokine staining (ICS) assay—For the intracellular cytokine analysis, 1×10^6 PBMCs per well were stimulated in the presence of $DENV_{pep}$ (2.5 μg/mL) or an equimolar amount of DMSO (vehicle control) in a 96-well U bottom plate for 6 h in standard culture conditions. GolgiPlug containing brefeldin A (BD Biosciences) was added to the cells 2 h after $DENV_{pep}$ addition. For polyclonal stimulation of PBMCs, 0.5×10^6 cells were stimulated with PMA (25 ng/mL; Sigma–Aldrich) and ionomycin (1 μg/mL; Sigma–Aldrich) in the presence of GolgiPlug containing brefeldin A for 4 h. After incubation, the cells were stained with surface antibodies and intracellular cytokine antibodies following the protocol described in the “Flow cytometry” section. The antibodies used in the ICS assay are listed in Table S7C. In another experiment analyzing IL-21 and GZMB in FACS-sorted $CXCR5^-PD\text{-}1^+$ $CD4^+$ T cells, 6×10^4 T cells per well were cocultured with $CD14^+$ monocytes at a 1:2 ratio and polyclonally activated with staphylococcal enterotoxin B (SEB; Sigma–Aldrich) at 1 μg/mL for 48 h. After activation, the cells were stimulated with PMA and ionomycin in the presence of GolgiPlug containing brefeldin A for 4 h. The cells were stained with intracellular cytokine antibodies (against human CD40L, IFN-γ, IL-21 and GZMB) as previously described. The antibodies used in this study are listed in Table S7C.

ELISPOT and Fluorospot assays—ELISPOT was performed to detect IL-21-secreting cells among FACS-sorted $CD45RO^+CXCR5^+$ and $CD45RO^+CXCR5^-$ $CD4^+$ T cells. An ELISPOT plate (MSIPS4510; Millipore) was charged with 35% ethanol (Merck Millipore) and coated with the mAb MT216G (10 μg/mL; Mabtech) overnight at 4°C. The plate was washed and blocked with AIM-V medium containing 10% FBS for at least 30 min at room temperature (RT). $CD4^+$ T cells (2×10^4 cells per well) were cocultured with a pool of $CD20^+$ B cells and $CD14^+$ and $CD16^+$ monocytes (4×10^4 cells per well) in AIM-V medium. The cells were stimulated with $DENV_{pep}$ (2 μg/mL) or an equimolar amount of DMSO for 24 h under standard culture conditions. For polyclonal stimulation, cells were stimulated with SEB (1 μg/mL). The plate was washed 5 times with PBS and incubated with the mAb MT21.3 m-biotin (0.25 mg/mL; Mabtech) for 2 h at RT. After incubation, the plate was developed according to the Human IL-21 ELISPOT (3540-2A) manufacturer’s instructions. For FluoroSpot detection of IFN-γ-secreting cells, an IPFL plate (Mabtech) was charged with 35% ethanol and coated with the mAb 1-D1K (15 μg/mL; Mabtech) overnight. The plate was blocked, and the cells were cultured as described above. Spots were detected with the BAM-conjugated mAb 7-B6-1 (Mabtech) diluted 1:200. The reaction was developed following the kit protocol (FS-0107; Mabtech). IL-21 and IFN-γ spot counts were read on a vSpot Spectrum ELISPOT/FluoroSpot reader (AID GmbH) using AID Elispot software v7.x.

DENV-reactive IgG ELISA—An in-house-developed indirect ELISA was performed to measure DENV-reactive IgG antibodies in the plasma samples. F-bottom immuno-96-well plates (Thermo Fisher) were coated with 1 μg/mL recombinant DENV-2 NS1 protein or

DENV-2 virus-like particles consisting of prM, M and E proteins (Native Antigen, UK) overnight at 4°C. The next day, the plates were washed 3 times with PBS containing 0.05% Tween 20 (Sigma–Aldrich) and blocked with 3% skim milk powder (SMP; Himedia) in PBS supplemented with 0.05% Tween 20 for 2 h at RT. The plasma was diluted in PBS containing 1% SMP and 0.05% Tween 20 starting at a dilution of 1:1000, followed by a serial dilution of 1:3. Diluted plasma was subsequently added to the plates and incubated for 1.5 h. The plasma was heat inactivated at 56°C for 30 min before being added to the plates. After incubation, the plates were washed 5 times with PBS-0.05% Tween 20, and secondary goat anti-human IgG antibody conjugated with HRP (Southern Biotech) was added at a 1:4000 dilution and incubated for 1 h. The plates were washed 5 times with PBS-0.05% Tween 20. The reaction mixture was incubated with OPD peroxidase substrate (Sigma) for 10 min at RT in the dark. The reaction was stopped with 2 N hydrochloric acid (HCl; Merck Millipore). The plates were read on a MultiskanGO ELISA reader (Thermo Fisher Scientific) at 492 nm using SkanIt Software v6.1. The optical density (OD) values of the samples were background-subtracted from the blank OD values of PBS-1% SMP and 0.05% Tween 20.

CXCL13 ELISA—A human CXCL13/BLC/BCA-1 Quantikine ELISA Kit (R&D Systems) was used to measure the CXCL13 cytokine concentration in plasma samples as a circulating GC marker. Freshly thawed plasma samples were subjected to this assay according to the manufacturer's instructions.

FRNT neutralization assay—DENV neutralization titer was determined by focus reduction neutralization titer (FRNT) assay. Briefly, Vero (ATCC# CCL-81) cells were seeded at 20,000 per well in 96 white flat-bottom plate (Nunc # 136101) and incubated overnight at 37°C with 5% CO_2. Next day, plasma samples were heat inactivated at 56°C for 30 min. Further, 3-fold serial dilutions (starting dilution 1:10) of plasma samples were prepared and mixed with DENV-2 virus with 100–150 FFU, and the mixture was incubated for 1 h at 37°C. After incubation, cell monolayers were washed with 1x DPBS and a mixture was added to the cell monolayer and incubated for 90 min at 37°C. The mixture was removed and replaced with 1% Carboxymethyl cellulose (CMC) overlay media and incubated for 48 h at 37°C with 5% CO_2. Cells were fixed with 4% paraformaldehyde (Electron microscopy #50-980-493) for 30 min at RT. Later, cells were washed with 1x DPBS, blocked and permeabilized using blocking permeabilization buffer (0.1% BSA plus 0.1% saponin) for 30 min at RT. The cells were subsequently stained with the primary antibody 4G2 (2 μg/mL, purified from 4G2 hybridoma) for 2 h at RT. Cells were washed with 1x DPBS and stained with secondary antibody anti-mouse HRP conjugated at 1:2000 dilution (Southern Biotech #1030-05) for 1 h at RT. Following incubation, cells were washed with 1x DPBS, focus was developed using True Blue Substrate (KPL# 5510-0030), and spots were read on AID GmbH ELISPOT reader using AID Elispot software v7.x. Neutralization 50 was calculated based on non-linear regression analysis using Prism v.10 (GraphPad software).

Cytokine multiplex bead assay—Cytokines in the plasma samples were quantified using a human cytokine 48-plex screening panel (Bio-Plex; Bio-Rad). The plasma

samples were stored at −80°C. The cytokine immunoassay was performed following the manufacturer's instructions. The plates were read on a Bio-Plex 200 reader (Bio-Rad) using Bio-Plex Manager v6.2.

Lymphoid tissue processing—Lymphoid tissue was processed to generate a single-cell suspension on the same day as the tissue sample was excised. The tissue was transferred to a 90 mm Petri dish containing warm complete RPMI medium supplemented with 10% FBS and 1% Pen-Strep (Gibco). Excess fat and connective tissue were removed, and the tissue was then minced manually using dissecting scalpels to obtain ~1–2 mm^3 pieces. The minced tissue suspension was passed through a 70 μm cell strainer (Corning), and the larger remaining cells were triturated into fine pieces using a 2 mL syringe piston. The minced tissue suspension was centrifuged at 100x g at RT for 10 min. The cells were treated with ACK lysis buffer (Gibco) to remove red cell contamination and passed through a 40 μm cell strainer to obtain a uniform single-cell suspension. The cells were again centrifuged at 400x g at RT for 10 min and resuspended in complete RPMI medium. Cell count and viability were assessed as described previously. The cells were cryopreserved in several aliquots in FBS containing 10% (v/v) DMSO and stored in liquid nitrogen for later analysis.

Autologous T-B cocultures—B cell helper function was assessed by an efficient *ex vivo* T-B coculture setting previously validated in SARS-CoV-2-specific memory $CD4^+$ T cells by our group.[32] Briefly, FACS-generated purified $CD4^+$ T cells (6×10^4 cells/well) were cocultured with autologous $CD20^+$ B cells (6×10^4 cells/well) in the presence of autologous $CD14^+$ monocytes (3×10^4 cells/well) in AIM-V medium in a 96-well U bottom plate for 9 days under standard culture conditions. $CD4^+$ T cells were stimulated with 1 μg/mL $DENV_{pep}$ or an equimolar amount of DMSO (vehicle control), and no exogenous cytokines or culture media were added/replaced throughout the duration of cocultures. For blocking experiments, IL-21R-Fc (5 μg/mL; R&D Systems), the α-IL-10 mAb (5 μg/mL; R&D Systems) and the α-IL-4 mAb (10 μg/mL; R&D Systems) were added to $DENV_{pep}$-stimulated cocultures. After 9 days of coculture, viable cells were counted using a LUNA-FL cell counter, and plasmablast phenotyping was performed via flow cytometry. The antibodies used in the coculture assay are listed in Table S7C. The supernatants were collected from the cocultures and stored in aliquots at −20°C. DENV-reactive IgG antibodies (anti-NS1 and anti-prM/M/E) were detected in the undiluted supernatants via an in-house developed ELISA method as previously described.

Single-cell RNAseq and TCRseq assays (10x genomics)—For single-cell RNAseq and TCRseq analysis, cryopreserved PBMCs from 3 acute patients with dengue were thawed and processed as described previously. The cells were washed with 20 mL of PBS-2 mM EDTA buffer. A total of 3×10^6 PBMCs were blocked with 10% heat-inactivated human plasma by incubating for 10 min at 4°C. The cells were then surface stained with fluorochrome-tagged and TotalSeq-C (BioLegend) anti-human antibodies, as listed in Tables S7B and S7D, for 1 h at 4°C according to the manufacturer's instructions. PBMCs from each patient were also stained with anti-human Hashtag antibodies (BioLegend) before pooling. For FACS sorting of activated $CD4^+$ T cells, $ICOS^+CD38^+$ cells were gated on $CD4^+$ T cells as shown in Figure 6A and collected in separate tubes with RPMI 1640

medium. FACS-sorted $ICOS^+CD38^+$ $CD4^+$ T cells from three patients were pooled together in equal numbers and resuspended at a density of 1100 cells/μL with >90% viability. The cells were processed for gel bead-in-emulsion (GEM) generation, barcoding and cDNA preparation (10x Genomics) according to the manufacturer's recommendation. Single-cell RNA sequencing library preparation was performed using Chromium Next GEM Single-Cell 5′ Reagent Kit v2.0 (Dual Index) with immune profiling (VDJ) and cell surface protein feature barcode technology (10x Genomics). The initial cDNA amplification was performed with 13 amplification cycles. After amplification, the cDNA pellet was used to amplify the VDJ T cell receptor (TCR), after which the VDJ library was prepared via 8 cycles of amplification; preparation of the 5′ gene expression library was performed via 14 cycles of amplification. A cell surface protein (CSP) library was generated from the amplified cDNA supernatant after 8 amplification cycles. The quality and concentration of the cDNA libraries were assessed using the 5200 Fragment Analyzer system (Agilent) with an Agilent DNF-474 HS NGS Fragment Kit and a Qubit 4.0 fluorometer (Thermo-Fisher) with a dsDNA HS assay kit according to the manufacturer's recommendations. In addition, the insert size of the library was determined using a TapeStation 4150 (Agilent) and an Agilent high-sensitivity D1000 ScreenTape assay. The three libraries were pooled in molar concentrations according to a sequencing depth of ~30,000 reads/cell for 5′ gene expression and ~5,000 reads/cell for the VDJ and CSP libraries and sequenced on an Illumina NovaSeq 6000 platform (150 bp, paired-end) with the following parameters: read1 – 26 cycles; read2 – 90 cycles; and i7 and i5 indexes - 10 cycles.

Single-cell transcriptome analysis—Single-cell RNA sequencing (FASTQ) data from the 5′ RNA expression, VDJ-TCR and CSP libraries were simultaneously processed using the *cellranger multi*pipeline of Cell Ranger software v7.0.1 (10x Genomics). Unique molecular identifier (UMI) counts were assigned to the cell barcodes and mapped to reference genomes: GRCh38-2020-A for RNA, GRCh38-alts-ensembl-7.0.0 for VDJ-TCR, and TotalSeq-C (BioLegend) feature barcodes for CSP to generate a filtered RNA/CSP count matrix and filtered VDJ-TCR contig annotations. To demultiplex the cells from all three patients, raw reads from the 5° RNA expression and multiplexing capture (CSP) libraries were again processed with a *cellranger multi*pipeline to generate a sample-filtered RNA count matrix for each sample. Cell barcodes from all three patients were assigned to their respective patient IDs, and unassigned or doublets were discarded during demultiplexing. Next, the demultiplexed filtered count data from all patients were merged and analyzed via the R platform-based Seurat v4.3.0 package. The low-quality cells and empty droplets/cell doublets were removed by filtering out the cells expressing ⟨ 1000 or > 50,000 UMIs, ⟨ 500 or > 7,500 genes, > 7% mitochondrial UMIs, or ⟨ 7% ribosomal UMIs. A total of 4,361 filtered cells were recovered (81.33%) for downstream analysis. The count data were log-transformed and normalized (by a factor of 10,000) per cell using the default settings in Seurat, and the 3000 most variable genes were selected by the variance stabilizing transformation (vst) method.[28] The top genes were subjected to scaling and centered after regressing out the following variables: UMIs, genes, mitochondrial percentage, cell cycle genes (differences in S and G2M scores calculated by the *CellCycleScoring* function) and other confounding factors, gene signatures of dissociation-induced stress[74] and hypoxia[75] calculated by the *AddModuleScore* function. Principal component analysis (PCA) was

subsequently performed, and the top 30 principal components (PCs) were selected based on the standard deviation of the PCs in the "elbow plot". Clustering was performed using the *FindNeighbors* and *FindClusters* functions[76] with the default settings in Seurat and a resolution of 0.8. Visualizing the clusters via the UMAP approach resulted in clustering of the cells in a highly donor-specific manner. To minimize donor-based bias in clustering, data integration was performed using an anchor-based CCA method.[28] For CSP expression, filtered CSP count data for 4,361 filtered cells were assembled via the same Seurat procedure. The CSP count data were normalized using the centered log-ratio (CLR) method. For visualization of the normalized data, UMAP plots, feature plots, scatterplots, and violin plots were generated using visualization methods in Seurat.

Differential gene expression and GSEA—Differential gene expression analysis between two clusters or cell groups was performed by the *FindMarkers* function of the Seurat package, and the Model-based Analysis of Single-cell Transcriptomics (MAST) test parameter was applied.[67] A gene was considered differentially expressed when the Benjamini–Hochberg (BH) adjusted p value was ⟨0.05 and the $\log_2$|fold change| was > 0.25. Graphical visualization of DEGs, such as heatmaps, dot plots, and volcano plots, was performed using Seurat functions or ggplot2. Gene set enrichment analysis (GSEA) scores were calculated by the *fgsea* package for the cluster-enriched ranked gene sets.[68] The signature gene sets used for GSEA of cytotoxic CD4[77] and interferon response[78] are given in Table S6C.

Single-cell trajectory analysis—Monocle3 v1.3.1[69] was used to construct a branched trajectory through the cells based on the normalized count data from Seurat analysis. The cell trajectory was projected on a single partition of cells from all UMAP clusters generated in Seurat.

Single-cell TCR clonotype analysis—Filtered VDJ-TCR contig annotations were previously obtained using the *cellranger multi* pipeline in Cell Ranger v7.0.1 software (10x Genomics). VDJ-TCR annotations were processed with the scRepertoire package[70] (v1.10.0) to combine the TCR genes from the same cell barcodes. Unique TCR clonotypes were then counted and aggregated into RNA/CSP count data using the *combineExpression* function of the scRepertoire. A total of 3,935 cells out of 4,361 cells were recovered for clonotype analysis. Cells with more than 1 clone (clonal size > 1) were called clonally expanded, and their clonal sizes, single, small, medium, large, and hyperexpandable, were visualized on the UMAP plot. Clonal overlap of cells in two or more clusters was depicted using the tool circlize[71] or UpSetR.[72]

QUANTIFICATION AND STATISTICAL ANALYSIS

The data processing, methods and codes used are described in the respective sections of the Methods. The statistical details of the experiments are indicated in the respective Figure legends or methods. All the statistical analyses were performed using GraphPad Prism software v.10. The data were plotted in scatterplots and are presented as the median ± interquartile range (IQR). The data plotted in bar plots are expressed as the mean ± standard deviation of the mean (SEM). Statistical comparisons were performed using two-tailed

Student's t tests, nonparametric tests, Mann–Whitney U tests, or Wilcoxon signed-rank tests, with a p value of $\langle 0.05$ indicating statistical significance. Multiple comparisons were performed using ANOVA or nonparametric tests, the Friedman test for matched comparisons or the Kruskal–Wallis test for unmatched comparisons. The specific p values are depicted in the respective Figure panels.

Supplementary Material

Refer to Web version on PubMed Central for supplementary material.

ACKNOWLEDGMENTS

We are thankful to the participants for their generous support of this study. This work was financially supported by SERB, a DST grant (ECR/2016/001814), and a DBT grant (BT/NBM0099/02/18) to the NG and NII core grants. Further support was provided by NIH contract 75N9301900065 (to A.S. and D.W.) and NIH grant U01 (U01AI141995-03) to A.S.

REFERENCES

1. Bhatt S, Gething PW, Brady OJ, Messina JP, Farlow AW, Moyes CL, Drake JM, Brownstein JS, Hoen AG, Sankoh O, et al. (2013). The global distribution and burden of dengue. Nature 496, 504–507. 10.1038/nature12060. [PubMed: 23563266]
2. Guzman MG, Halstead SB, Artsob H, Buchy P, Farrar J, Gubler DJ, Hunsperger E, Kroeger A, Margolis HS, Martínez E, et al. (2010). Dengue: a continuing global threat. Nat. Rev. Microbiol. 8, S7–S16. 10.1038/nrmicro2460. [PubMed: 21079655]
3. Halstead SB, Nimmannitya S, and Cohen SN (1970). Observations related to pathogenesis of dengue hemorrhagic fever. IV. Relation of disease severity to antibody response and virus recovered. Yale J. Biol. Med. 42, 311–328. [PubMed: 5419206]
4. Halstead SB, Chow JS, and Marchette NJ (1973). Immunological enhancement of dengue virus replication. Nat. New Biol. 243, 24–26. [PubMed: 17319077]
5. Sangkawibha N, Rojanasuphot S, Ahandrik S, Viriyapongse S, Jatanasen S, Salitul V, Phanthumachinda B, and Halstead SB (1984). Risk factors in dengue shock syndrome: a prospective epidemiologic study in Rayong, Thailand. I. The 1980 outbreak. Am. J. Epidemiol. 120, 653–669. 10.1093/oxfordjournals.aje.a113932. [PubMed: 6496446]
6. Burke DS, Nisalak A, Johnson DE, and Scott RM (1988). A prospective study of dengue infections in Bangkok. Am. J. Trop. Med. Hyg. 38, 172–180. 10.4269/ajtmh.1988.38.172. [PubMed: 3341519]
7. Thein S, Aung MM, Shwe TN, Aye M, Zaw A, Aye K, Aye KM, and Aaskov J (1997). Risk factors in dengue shock syndrome. Am. J. Trop. Med. Hyg. 56, 566–572. 10.4269/ajtmh.1997.56.566. [PubMed: 9180609]
8. Dejnirattisai W, Jumnainsong A, Onsirisakul N, Fitton P, Vasanawathana S, Limpitikul W, Puttikhunt C, Edwards C, Duangchinda T, Supasa S, et al. (2010). Cross-reacting antibodies enhance dengue virus infection in humans. Science 328, 745–748. 10.1126/science.1185181. [PubMed: 20448183]
9. Guzman MG, Alvarez M, and Halstead SB (2013). Secondary infection as a risk factor for dengue hemorrhagic fever/dengue shock syndrome: an historical perspective and role of antibody-dependent enhancement of infection. Arch. Virol. 158, 1445–1459. 10.1007/s00705-013-1645-3. [PubMed: 23471635]
10. Salje H, Cummings DAT, Rodriguez-Barraquer I, Katzelnick LC, Lessler J, Klungthong C, Thaisomboonsuk B, Nisalak A, Weg A, Ellison D, et al. (2018). Reconstruction of antibody dynamics and infection histories to evaluate dengue risk. Nature 557, 719–723. 10.1038/s41586-018-0157-4. [PubMed: 29795354]
11. Anderson KB, Gibbons RV, Cummings DAT, Nisalak A, Green S, Libraty DH, Jarman RG, Srikiatkhachorn A, Mammen MP, Darunee B, et al. (2014). A shorter time interval between first

and second dengue infections is associated with protection from clinical illness in a school-based cohort in Thailand. J. Infect. Dis. 209, 360–368. 10.1093/infdis/jit436. [PubMed: 23964110]

12. Smith SA, Zhou Y, Olivarez NP, Broadwater AH, de Silva AM, and Crowe JE Jr. (2012). Persistence of circulating memory B cell clones with potential for dengue virus disease enhancement for decades following infection. J. Virol. 86, 2665–2675. 10.1128/JVI.06335-11. [PubMed: 22171265]
13. Hadinegoro SR, Arredondo-García JL, Capeding MR, Deseda C, Chotpitayasunondh T, Dietze R, Muhammad Ismail HIH, Reynales H, Limkittikul K, Rivera-Medina DM, et al. (2015). Efficacy and Long-Term Safety of a Dengue Vaccine in Regions of Endemic Disease. N. Engl. J. Med. 373, 1195–1206. 10.1056/NEJMoa1506223. [PubMed: 26214039]
14. Wrammert J, Onlamoon N, Akondy RS, Perng GC, Polsrila K, Chandele A, Kwissa M, Pulendran B, Wilson PC, Wittawatmongkol O, et al. (2012). Rapid and massive virus-specific plasmablast responses during acute dengue virus infection in humans. J. Virol. 86, 2911–2918. 10.1128/JVI.06075-11. [PubMed: 22238318]
15. Garcia-Bates TM, Cordeiro MT, Nascimento EJM, Smith AP, Soares de Melo KM, McBurney SP, Evans JD, Marques ETA Jr., and Barratt-Boyes SM (2013). Association between magnitude of the virus-specific plasmablast response and disease severity in dengue patients. J. Immunol. 190, 80–87. 10.4049/jimmunol.1103350. [PubMed: 23203929]
16. Simon-Loriere E, Duong V, Tawfik A, Ung S, Ly S, Casademont I, Prot M, Courtejoie N, Bleakley K, Buchy P, et al. (2017). Increased adaptive immune responses and proper feedback regulation protect against clinical dengue. Sci. Transl. Med. 9, eaal5088. 10.1126/scitranslmed.aal5088. [PubMed: 28855396]
17. Dejnirattisai W, Wongwiwat W, Supasa S, Zhang X, Dai X, Rouvinski A, Jumnainsong A, Edwards C, Quyen NTH, Duangchinda T, et al. (2015). A new class of highly potent, broadly neutralizing antibodies isolated from viremic patients infected with dengue virus. Nat. Immunol. 16, 170–177. 10.1038/ni.3058. [PubMed: 25501631]
18. Priyamvada L, Cho A, Onlamoon N, Zheng NY, Huang M, Kovalenkov Y, Chokephaibulkit K, Angkasekwinai N, Pattanapanyasat K, Ahmed R, et al. (2016). B Cell Responses during Secondary Dengue Virus Infection Are Dominated by Highly Cross-Reactive, Memory-Derived Plasmablasts. J. Virol. 90, 5574–5585. 10.1128/JVI.03203-15. [PubMed: 27030262]
19. Weiskopf D, Bangs DJ, Sidney J, Kolla RV, De Silva AD, de Silva AM, Crotty S, Peters B, and Sette A (2015). Dengue virus infection elicits highly polarized CX3CR1+ cytotoxic CD4+ T cells associated with protective immunity. Proc. Natl. Acad. Sci. USA 112, E4256–E4263. 10.1073/pnas.1505956112. [PubMed: 26195744]
20. Tian Y, Seumois G, De-Oliveira-Pinto LM, Mateus J, Herrera-de la Mata S, Kim C, Hinz D, Goonawardhana NDS, de Silva AD, Premawansa S, et al. (2019). Molecular Signatures of Dengue Virus-Specific IL-10/IFN-gamma Co-producing CD4 T Cells and Their Association with Dengue Disease. Cell Rep. 29, 4482–4495.e4. 10.1016/j.celrep.2019.11.098. [PubMed: 31875555]
21. Ueno H (2016). T follicular helper cells in human autoimmunity. Curr. Opin. Immunol. 43, 24–31. 10.1016/j.coi.2016.08.003. [PubMed: 27588918]
22. Crotty S (2019). T Follicular Helper Cell Biology: A Decade of Discovery and Diseases. Immunity 50, 1132–1148. 10.1016/j.immuni.2019.04.011. [PubMed: 31117010]
23. Haltaufderhyde K, Srikiatkhachorn A, Green S, Macareo L, Park S, Kalayanarooj S, Rothman AL, and Mathew A (2018). Activation of Peripheral T Follicular Helper Cells During Acute Dengue Virus Infection. J. Infect. Dis. 218, 1675–1685. 10.1093/infdis/jiy360. [PubMed: 29917084]
24. Mathew A, West K, Kalayanarooj S, Gibbons RV, Srikiatkhachorn A, Green S, Libraty D, Jaiswal S, and Rothman AL (2011). B cell responses during primary and secondary dengue virus infections in humans. J. Infect. Dis. 204, 1514–1522. 10.1093/infdis/jir607. [PubMed: 21930609]
25. Zompi S, Montoya M, Pohl MO, Balmaseda A, and Harris E (2012). Dominant cross-reactive B cell response during secondary acute dengue virus infection in humans. PLoS Neglected Trop. Dis. 6, e1568. 10.1371/journal.pntd.0001568.
26. Rouers A, Chng MHY, Lee B, Rajapakse MP, Kaur K, Toh YX, Sathiakumar D, Loy T, Thein TL, Lim VWX, et al. (2021). Immune cell phenotypes associated with disease severity and long-term neutralizing antibody titers after natural dengue virus infection. Cell Rep. Med. 2, 100278. 10.1016/j.xcrm.2021.100278. [PubMed: 34095880]

27. WHO (2009). Dengue: Guidelines for Diagnosis, Treatment, Prevention and Control: New Edition (WHO/TDR). https://iris.who.int/handle/10665/44188.
28. Stuart T, Butler A, Hoffman P, Hafemeister C, Papalexi E, Mauck WM 3rd, Hao Y, Stoeckius M, Smibert P, and Satija R (2019). Comprehensive Integration of Single-Cell Data. Cell 177, 1888–1902.e21. 10.1016/j.cell.2019.05.031. [PubMed: 31178118]
29. Grifoni A, Angelo MA, Lopez B, O'Rourke PH, Sidney J, Cerpas C, Balmaseda A, Silveira CGT, Maestri A, Costa PR, et al. (2017). Global Assessment of Dengue Virus-Specific CD4(+) T Cell Responses in Dengue-Endemic Areas. Front. Immunol. 8, 1309. 10.3389/fimmu.2017.01309. [PubMed: 29081779]
30. Alcon S, Talarmin A, Debruyne M, Falconar A, Deubel V, and Flamand M (2002). Enzyme-linked immunosorbent assay specific to Dengue virus type 1 nonstructural protein NS1 reveals circulation of the antigen in the blood during the acute phase of disease in patients experiencing primary or secondary infections. J. Clin. Microbiol. 40, 376–381. 10.1128/JCM.40.02.376-381.2002. [PubMed: 11825945]
31. Havenar-Daughton C, Lindqvist M, Heit A, Wu JE, Reiss SM, Kendric K, Bélanger S, Kasturi SP, Landais E, Akondy RS, et al. (2016). CXCL13 is a plasma biomarker of germinal center activity. Proc. Natl. Acad. Sci. USA 113, 2702–2707. 10.1073/pnas.1520112113. [PubMed: 26908875]
32. Ansari A, Sachan S, Jit BP, Sharma A, Coshic P, Sette A, Weiskopf D, and Gupta N (2022). An efficient immunoassay for the B cell help function of SARS-CoV-2-specific memory CD4(+) T cells. Cell Rep. Methods 2, 100224. 10.1016/j.crmeth.2022.100224.
33. Ettinger R, Sims GP, Fairhurst AM, Robbins R, da Silva YS, Spolski R, Leonard WJ, and Lipsky PE (2005). IL-21 induces differentiation of human naive and memory B cells into antibody-secreting plasma cells. J. Immunol. 175, 7867–7879. 10.4049/jimmunol.175.12.7867. [PubMed: 16339522]
34. Good KL, Bryant VL, and Tangye SG (2006). Kinetics of human B cell behavior and amplification of proliferative responses following stimulation with IL-21. J. Immunol. 177, 5236–5247. 10.4049/jimmunol.177.8.5236. [PubMed: 17015709]
35. Albrecht I, Niesner U, Janke M, Menning A, Loddenkemper C, Kühl AA, Lepenies I, Lexberg MH, Westendorf K, Hradilkova K, et al. (2010). Persistence of effector memory Th1 cells is regulated by Hopx. Eur. J. Immunol. 40, 2993–3006. 10.1002/eji.201040936. [PubMed: 21061432]
36. Baaten BJG, Li CR, Deiro MF, Lin MM, Linton PJ, and Bradley LM (2010). CD44 regulates survival and memory development in Th1 cells. Immunity 32, 104–115. 10.1016/j.immuni.2009.10.011. [PubMed: 20079666]
37. Freeley S, Cardone J, Günther SC, West EE, Reinheckel T, Watts C, Kemper C, and Kolev MV (2018). Asparaginyl Endopeptidase (Legumain) Supports Human Th1 Induction via Cathepsin L-Mediated Intracellular C3 Activation. Front. Immunol. 9, 2449. 10.3389/fimmu.2018.02449. [PubMed: 30405635]
38. Shin H, and Iwasaki A (2013). Tissue-resident memory T cells. Immunol. Rev. 255, 165–181. 10.1111/imr.12087. [PubMed: 23947354]
39. Woodruff MC, Ramonell RP, Nguyen DC, Cashman KS, Saini AS, Haddad NS, Ley AM, Kyu S, Howell JC, Ozturk T, et al. (2020). Extrafollicular B cell responses correlate with neutralizing antibodies and morbidity in COVID-19. Nat. Immunol. 21, 1506–1516. 10.1038/s41590-020-00814-z. [PubMed: 33028979]
40. St John AL, and Rathore APS (2019). Adaptive immune responses to primary and secondary dengue virus infections. Nat. Rev. Immunol. 19, 218–230. 10.1038/s41577-019-0123-x. [PubMed: 30679808]
41. Sangkaew S, Ming D, Boonyasiri A, Honeyford K, Kalayanarooj S, Yacoub S, Dorigatti I, and Holmes A (2021). Risk predictors of progression to severe disease during the febrile phase of dengue: a systematic review and meta-analysis. Lancet Infect. Dis. 21, 1014–1026. 10.1016/S1473-3099(20)30601-0. [PubMed: 33640077]
42. Jayathilaka D, Gomes L, Jeewandara C, Jayarathna GSB, Herath D, Perera PA, Fernando S, Wijewickrama A, Hardman CS, Ogg GS, and Malavige GN (2018). Role of NS1 antibodies in the pathogenesis of acute secondary dengue infection. Nat. Commun. 9, 5242. 10.1038/s41467-018-07667-z. [PubMed: 30531923]

43. Falconar AK (1997). The dengue virus nonstructural-1 protein (NS1) generates antibodies to common epitopes on human blood clotting, integrin/adhesin proteins and binds to human endothelial cells: potential implications in haemorrhagic fever pathogenesis. Arch. Virol. 142, 897–916. 10.1007/s007050050127. [PubMed: 9191856]
44. Lin CF, Lei HY, Shiau AL, Liu CC, Liu HS, Yeh TM, Chen SH, and Lin YS (2003). Antibodies from dengue patient sera cross-react with endothelial cells and induce damage. J. Med. Virol. 69, 82–90. 10.1002/jmv.10261. [PubMed: 12436482]
45. Chuang YC, Lin YS, Liu HS, and Yeh TM (2014). Molecular mimicry between dengue virus and coagulation factors induces antibodies to inhibit thrombin activity and enhance fibrinolysis. J. Virol. 88, 13759–13768. 10.1128/JVI.02166-14. [PubMed: 25231318]
46. Katzelnick LC, Gresh L, Halloran ME, Mercado JC, Kuan G, Gordon A, Balmaseda A, and Harris E (2017). Antibody-dependent enhancement of severe dengue disease in humans. Science 358, 929–932. 10.1126/science.aan6836. [PubMed: 29097492]
47. Appanna R, Kg S, Xu MH, Toh YX, Velumani S, Carbajo D, Lee CY, Zuest R, Balakrishnan T, Xu W, et al. (2016). Plasmablasts During Acute Dengue Infection Represent a Small Subset of a Broader Virus-specific Memory B Cell Pool. EBioMedicine 12, 178–188. 10.1016/j.ebiom.2016.09.003. [PubMed: 27628668]
48. Vella LA, Buggert M, Manne S, Herati RS, Sayin I, Kuri-Cervantes L, Bukh Brody I, O'Boyle KC, Kaprielian H, Giles JR, et al. (2019). T follicular helper cells in human efferent lymph retain lymphoid characteristics. J. Clin. Investig. 129, 3185–3200. 10.1172/JCI125628. [PubMed: 31264971]
49. Ellebedy AH, Jackson KJL, Kissick HT, Nakaya HI, Davis CW, Roskin KM, McElroy AK, Oshansky CM, Elbein R, Thomas S, et al. (2016). Defining antigen-specific plasmablast and memory B cell subsets in human blood after viral infection or vaccination. Nat. Immunol. 17, 1226–1234. 10.1038/ni.3533. [PubMed: 27525369]
50. Asashima H, Mohanty S, Comi M, Ruff WE, Hoehn KB, Wong P, Klein J, Lucas C, Cohen I, Coffey S, et al. (2023). PD-1(high)CXCR5(−) CD4(+) peripheral helper T cells promote CXCR3(+) plasmablasts in human acute viral infection. Cell Rep. 42, 111895. 10.1016/j.celrep.2022.111895. [PubMed: 36596303]
51. Djuretic IM, Levanon D, Negreanu V, Groner Y, Rao A, and Ansel KM (2007). Transcription factors T-bet and Runx3 cooperate to activate Ifng and silence Il4 in T helper type 1 cells. Nat. Immunol. 8, 145–153. 10.1038/ni1424. [PubMed: 17195845]
52. Oestreich KJ, and Weinmann AS (2012). Transcriptional mechanisms that regulate T helper 1 cell differentiation. Curr. Opin. Immunol. 24, 191–195. 10.1016/j.coi.2011.12.004. [PubMed: 22240120]
53. Choi J, and Crotty S (2021). Bcl6-Mediated Transcriptional Regulation of Follicular Helper T cells (T(FH)). Trends Immunol. 42, 336–349. 10.1016/j.it.2021.02.002. [PubMed: 33663954]
54. Del Alcazar D, Wang Y, He C, Wendel BS, Del Río-Estrada PM, Lin J, Ablanedo-Terrazas Y, Malone MJ, Hernandez SM, Frank I, et al. (2019). Mapping the Lineage Relationship between CXCR5(+) and CXCR5(−) CD4(+) T Cells in HIV-Infected Human Lymph Nodes. Cell Rep. 28, 3047–3060.e7. 10.1016/j.celrep.2019.08.037. [PubMed: 31533030]
55. Rao DA, Gurish MF, Marshall JL, Slowikowski K, Fonseka CY, Liu Y, Donlin LT, Henderson LA, Wei K, Mizoguchi F, et al. (2017). Pathologically expanded peripheral T helper cell subset drives B cells in rheumatoid arthritis. Nature 542, 110–114. 10.1038/nature20810. [PubMed: 28150777]
56. Caielli S, Veiga DT, Balasubramanian P, Athale S, Domic B, Murat E, Banchereau R, Xu Z, Chandra M, Chung CH, et al. (2019). A CD4(+) T cell population expanded in lupus blood provides B cell help through interleukin-10 and succinate. Nat. Med. 25, 75–81. 10.1038/s41591-018-0254-9. [PubMed: 30478422]
57. Christophersen A, Lund EG, Snir O, Solà E, Kanduri C, Dahal-Koirala S, Zühlke S, Molberg Ø, Utz PJ, Rohani-Pichavant M, et al. (2019). Distinct phenotype of CD4(+) T cells driving celiac disease identified in multiple autoimmune conditions. Nat. Med. 25, 734–737. 10.1038/s41591-019-0403-9. [PubMed: 30911136]
58. Muskardin TLW, and Niewold TB (2018). Type I interferon in rheumatic diseases. Nat. Rev. Rheumatol. 14, 214–228. 10.1038/nrrheum.2018.31. [PubMed: 29559718]

59. Sumida TS, Dulberg S, Schupp JC, Lincoln MR, Stillwell HA, Axisa PP, Comi M, Unterman A, Kaminski N, Madi A, et al. (2022). Type I interferon transcriptional network regulates expression of coinhibitory receptors in human T cells. Nat. Immunol. 23, 632–642. 10.1038/s41590-022-01152-y. [PubMed: 35301508]
60. Elsner RA, and Shlomchik MJ (2020). Germinal Center and Extrafollicular B Cell Responses in Vaccination, Immunity, and Autoimmunity. Immunity 53, 1136–1150. 10.1016/j.immuni.2020.11.006. [PubMed: 33326765]
61. Jenks SA, Cashman KS, Zumaquero E, Marigorta UM, Patel AV, Wang X, Tomar D, Woodruff MC, Simon Z, Bugrovsky R, et al. (2018). Distinct Effector B Cells Induced by Unregulated Toll-like Receptor 7 Contribute to Pathogenic Responses in Systemic Lupus Erythematosus. Immunity 49, 725–739.e6. 10.1016/j.immuni.2018.08.015. [PubMed: 30314758]
62. Lin CF, Wan SW, Cheng HJ, Lei HY, and Lin YS (2006). Autoimmune pathogenesis in dengue virus infection. Viral Immunol. 19, 127–132. 10.1089/vim.2006.19.127. [PubMed: 16817755]
63. Popescu M, Cabrera-Martinez B, and Winslow GM (2019). TNF-alpha Contributes to Lymphoid Tissue Disorganization and Germinal Center B Cell Suppression during Intracellular Bacterial Infection. J. Immunol. 203, 2415–2424. 10.4049/jimmunol.1900484. [PubMed: 31570507]
64. Rivino L, Kumaran EA, Thein TL, Too CT, Gan VCH, Hanson BJ, Wilder-Smith A, Bertoletti A, Gascoigne NRJ, Lye DC, et al. (2015). Virus-specific T lymphocytes home to the skin during natural dengue infection. Sci. Transl. Med. 7, 278ra35. 10.1126/scitranslmed.aaa0526.
65. Szabo PA, Miron M, and Farber DL (2019). Location, location, location: Tissue resident memory T cells in mice and humans. Sci. Immunol. 4, eaas9673. 10.1126/sciimmunol.aas9673. [PubMed: 30952804]
66. Xiong Y, Piao W, Brinkman CC, Li L, Kulinski JM, Olivera A, Cartier A, Hla T, Hippen KL, Blazar BR, et al. (2019). CD4 T cell sphingosine 1-phosphate receptor (S1PR)1 and S1PR4 and endothelial S1PR2 regulate afferent lymphatic migration. Sci. Immunol. 4, eaav1263. 10.1126/sciimmunol.aav1263. [PubMed: 30877143]
67. Finak G, McDavid A, Yajima M, Deng J, Gersuk V, Shalek AK, Slichter CK, Miller HW, McElrath MJ, Prlic M, et al. (2015). MAST: a flexible statistical framework for assessing transcriptional changes and characterizing heterogeneity in single-cell RNA sequencing data. Genome Biol. 16, 278. 10.1186/s13059-015-0844-5. [PubMed: 26653891]
68. Korotkevich G, Sukhov V, Budin N, Shpak B, Artyomov MN, and Sergushichev A (2021). Fast gene set enrichment analysis. Preprint at bioRxiv, 060012. 10.1101/060012.
69. Trapnell C, Cacchiarelli D, Grimsby J, Pokharel P, Li S, Morse M, Lennon NJ, Livak KJ, Mikkelsen TS, and Rinn JL (2014). The dynamics and regulators of cell fate decisions are revealed by pseudotemporal ordering of single cells. Nat. Biotechnol. 32, 381–386. 10.1038/nbt.2859. [PubMed: 24658644]
70. Borcherding N, Bormann NL, and Kraus G (2020). scRepertoire: An R-based toolkit for single-cell immune receptor analysis. F1000Res. 9, 47. 10.12688/f1000research.22139.2. [PubMed: 32789006]
71. Gu Z, Gu L, Eils R, Schlesner M, and Brors B (2014). circlize Implements and enhances circular visualization in R. Bioinformatics 30, 2811–2812. 10.1093/bioinformatics/btu393. [PubMed: 24930139]
72. Conway JR, Lex A, and Gehlenborg N (2017). UpSetR: an R package for the visualization of intersecting sets and their properties. Bioinformatics 33, 2938–2940. 10.1093/bioinformatics/btx364. [PubMed: 28645171]
73. Dan JM, Lindestam Arlehamn CS, Weiskopf D, da Silva Antunes R, Havenar-Daughton C, Reiss SM, Brigger M, Bothwell M, Sette A, and Crotty S (2016). A Cytokine-Independent Approach To Identify Antigen-Specific Human Germinal Center T Follicular Helper Cells and Rare Antigen-Specific CD4+ T Cells in Blood. J. Immunol. 197, 983–993. 10.4049/jimmunol.1600318. [PubMed: 27342848]
74. van den Brink SC, Sage F, Vértesy Á, Spanjaard B, Peterson-Maduro J, Baron CS, Robin C, and van Oudenaarden A (2017). Single-cell sequencing reveals dissociation-induced gene expression in tissue subpopulations. Nat. Methods 14, 935–936. 10.1038/nmeth.4437. [PubMed: 28960196]

75. Buffa FM, Harris AL, West CM, and Miller CJ (2010). Large meta-analysis of multiple cancers reveals a common, compact and highly prognostic hypoxia metagene. Br. J. Cancer 102, 428–435. 10.1038/sj.bjc.6605450. [PubMed: 20087356]

76. Xu C, and Su Z (2015). Identification of cell types from single-cell transcriptomes using a novel clustering method. Bioinformatics 31, 1974–1980. 10.1093/bioinformatics/btv088. [PubMed: 25805722]

77. Patil VS, Madrigal A, Schmiedel BJ, Clarke J, O'Rourke P, de Silva AD, Harris E, Peters B, Seumois G, Weiskopf D, et al. (2018). Precursors of human CD4(+) cytotoxic T lymphocytes identified by single-cell transcriptome analysis. Sci. Immunol. 3, eaan8664. 10.1126/sciimmunol.aan8664. [PubMed: 29352091]

78. Seumois G, Ramírez-Suástegui C, Schmiedel BJ, Liang S, Peters B, Sette A, and Vijayanand P (2020). Single-cell transcriptomic analysis of allergen-specific T cells in allergy and asthma. Sci Immunol 5, eaba6087. 10.1126/sciimmunol.aba6087. [PubMed: 32532832]

Highlights

- $CXCR5^{-}PD\text{-}1^{+}CD4^{+}$ cells accumulate in severe dengue, featuring “helper” and “cytotoxic” subsets
- $IL\text{-}21^{+}$ helper T cells distinct from Tfh cells drive B cell help in dengue via IL-21 signaling
- Peripheral $IL\text{-}21^{+}$ helper cells acquire memory and home to tissues
- $IL\text{-}21^{+}$ helper T cells drive humoral response in dengue through extrafollicular niche

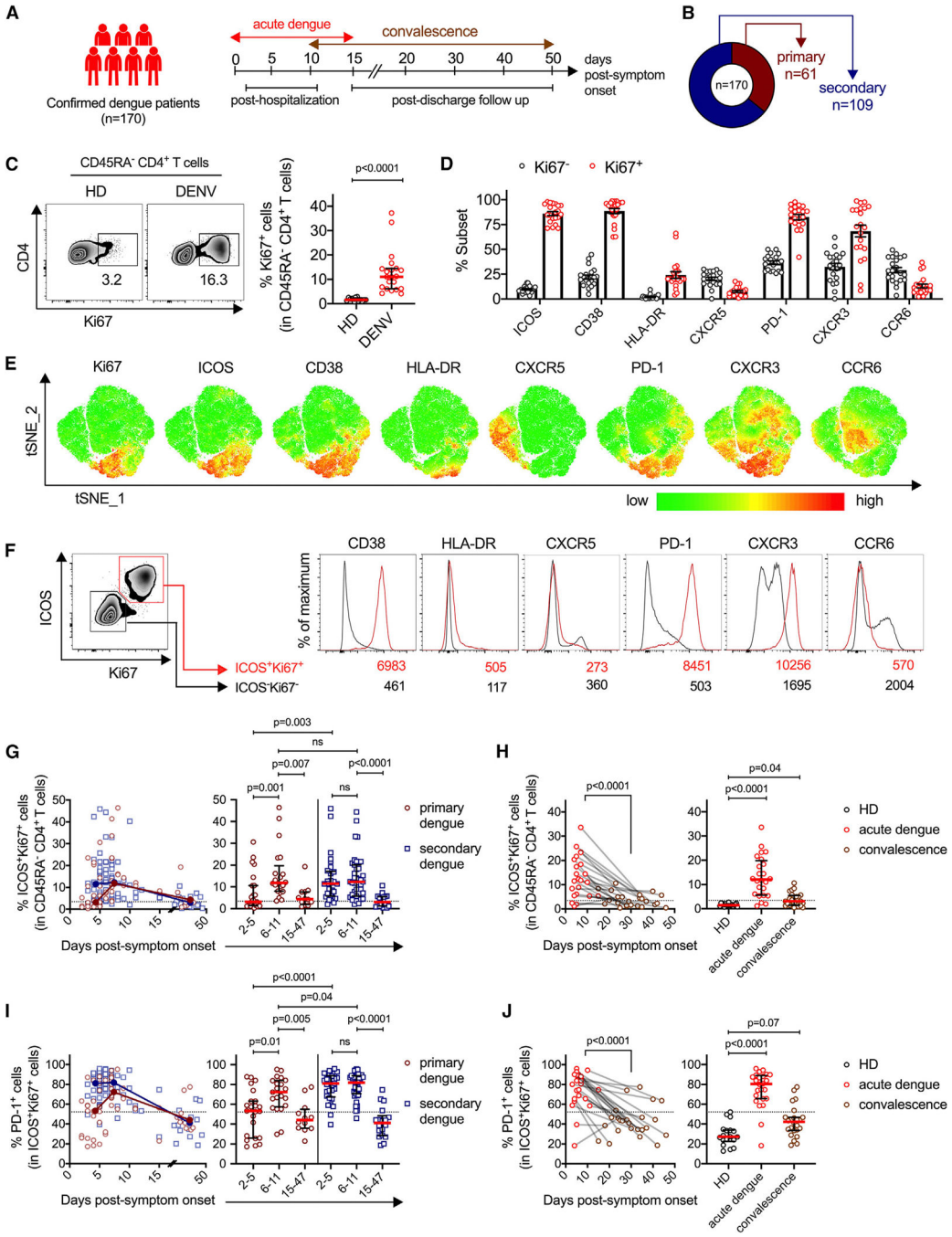

Figure 1. Phenotypic analyses of activated CD4$^+$ T cells in the blood of acute dengue

(A) Scheme depicting the time frame of blood sampling during acute and convalescent dengue.

(B) Proportion of primary and secondary infections in the study cohort of acute dengue (DENV).

(C) Representative intranuclear Ki67 staining of CD45RA$^-$CD4$^+$ T cells. A scatter dotplot shows the frequency of Ki67$^+$ cells in healthy donors (HDs) (n = 13) and patients (n = 21).

(D) Scatter barplot shows the frequency of Ki67-positive and Ki67-negative T cells with significant ($p < 0.0001$) differential expression. Data are presented as mean ± SEM.
(E) t-SNE analysis showing the coexpression of the markers shown in (D) in equally concatenated CD45RA^{-}CD4^{+} T cells from nine DENV samples.
(F) Example fluorescence-activated cell sorting (FACS) plot showing the costaining of ICOS and Ki67 in CD45RA^{-}CD4^{+} T cells, and histogram plots showing the geometric MFI of the markers in double-positive (red) and double-negative (black) cells.
(G) Scatter dotplots displaying the frequency of activated (ICOS^{+}Ki67^{+}) CD4^{+} T cells at continuous and grouped time points from cross-sectional cohorts of primary ($n = 56$) and secondary ($n = 86$) dengue.
(H) Longitudinal analysis of paired acute and convalescent samples ($n = 24$) showing the frequency of activated CD4^{+} T cells in comparison with that in HD samples ($n = 18$).
(I and J) Scatter dotplots quantifying the frequency of PD-1-expressing cells among activated CD4^{+} T cells in (I) cross-sectional and (J) longitudinal paired acute and convalescent samples as shown in (G) and (H), respectively.
Statistics: (C) Mann-Whitney test, (D) multiple t tests and correction by Holm-Sidak method, (G–J) Kruskal-Wallis test followed by Dunn’s multiple comparisons test, (H and J) Wilcoxon matched-pairs signed rank test. ns, not significant. Data are shown as median ± interquartile range (IQR). See also Figure S1.

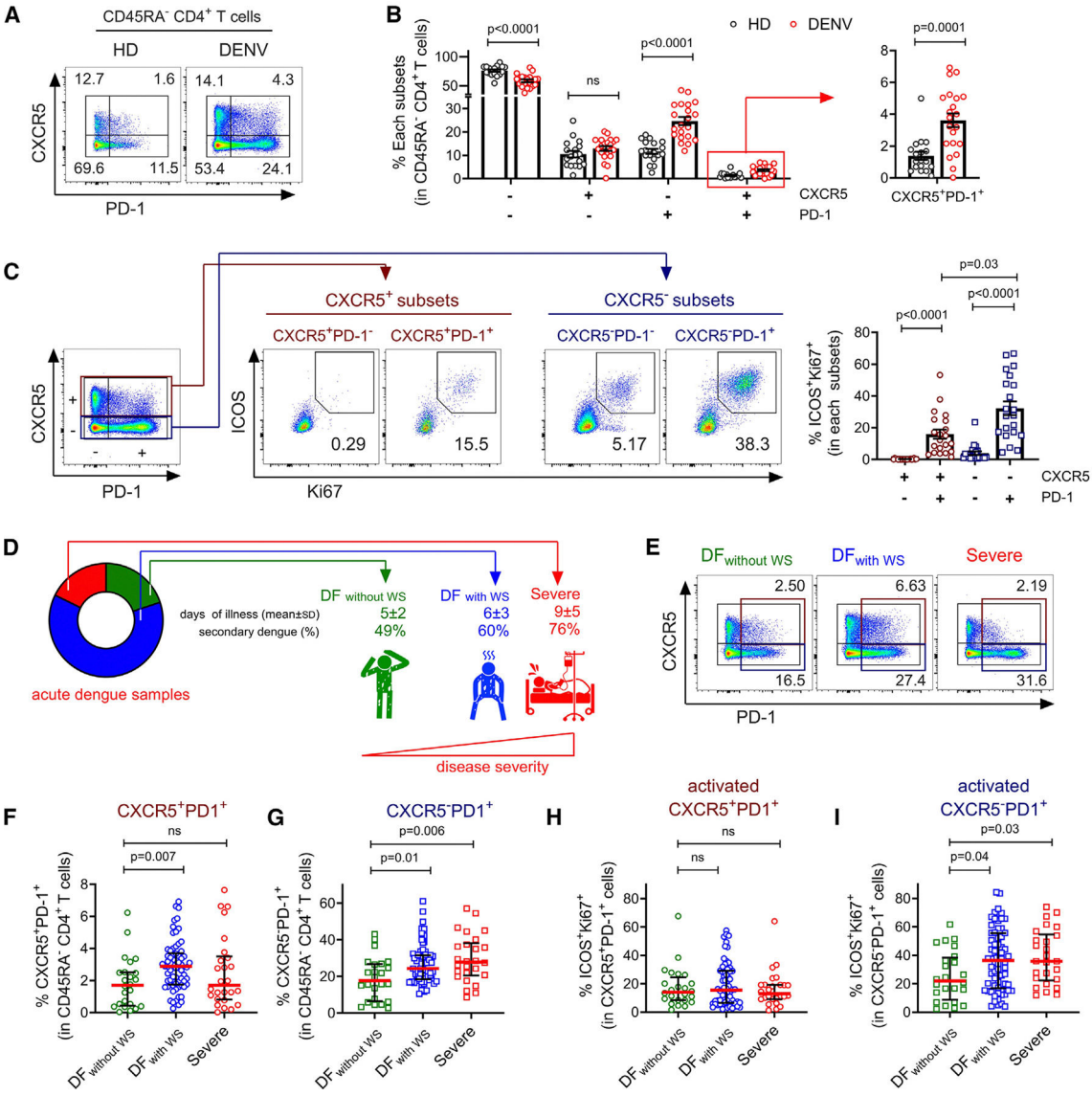

Figure 2. Activated CXCR5^{-}PD-1^{+}CD4^{+} T cells accumulate in patients with dengue with warning signs and severity

(A) Representative FACS plots showing the expression levels of CXCR5 and PD-1 on CD45RA^{-}CD4^{+} T cells.

(B) A scatter barplot was used to quantify the frequency of each indicated subset of CD45RA^{-}CD4^{+} T cells in HD (n = 18) and acute dengue virus (n = 21) samples. Data are presented as mean ± SEM.

(C) Representative FACS plots (left panels) and the frequency of activated (ICOS^{+}Ki67^{+}) T cells (right panel) within each of the four phenotypic subsets according to the expression of CXCR5 and PD-1. Data are shown as mean ± SEM.

(D) Graphical view of disease categorization of acute dengue samples with different degrees of severity: dengue fever (DF) without warning signs (WS), DF with WS, and severe. The frequency of secondary dengue within each of the categories is shown.

(E) Representative FACS plots showing the frequency of $CXCR5^{+}PD\text{-}1^{+}$ and $CXCR5^{-}PD\text{-}1^{+}CD4^{+}$ T cell subsets in DFs from patients without WS, DFs from patients with WS, and severe dengue (DENV) samples.

(F and G) Scatter dotplots quantifying the frequency of (F) $CXCR5^{+}PD\text{-}1^{+}$ and (G) $CXCR5^{-}PD\text{-}1^{+}$ subsets in DENV samples with worsening severity: DF without WS (n = 24), DF with WS (n = 66), and severe (n = 26).

(H and I) Frequencies of activated cells within the two indicated subsets (H) $CXCR5^{+}PD\text{-}1^{+}$ and (I) $CXCR5^{-}PD\text{-}1^{+}$, as shown in (F) and (G), respectively.

Statistics: (B) multiple t tests followed by Holm-Sidak method; (C) Friedman test followed by Dunn's multiple comparisons test; (F–I) Kruskal-Wallis test followed by Dunn's multiple comparisons test. ns, not significant. Data are presented as median ± IQR. See also Figure S2.

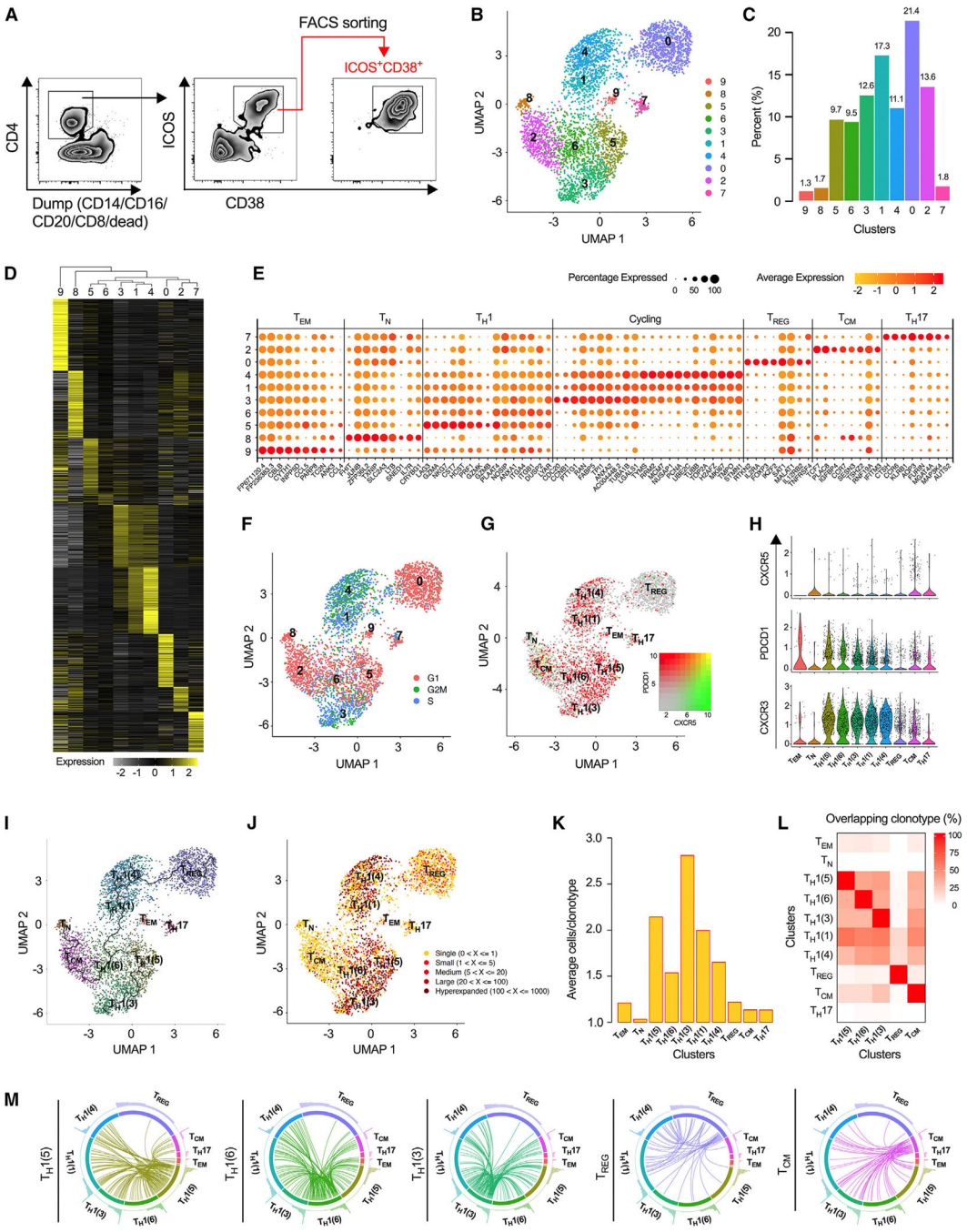

Figure 3. Single-cell RNA-seq and TCR-seq analyses of activated CD4$^+$ T cells from acute dengue revealed heterogeneity in the CXCR5$^-$PD-1$^+$ population

(A) Example gating scheme for FACS sorting of live activated CD4$^+$ T cells coexpressing ICOS and CD38 from acute dengue PBMCs.

(B) Single-cell RNA-seq transcriptome of sorted ICOS$^+$CD38$^+$CD4$^+$ T cells from patients (n = 3) with acute dengue. The plot shows the Seurat-based clustering of 4,361 cells displayed by UMAP.

(C) Barplot showing the percentages of Seurat clusters.

(D) Heatmap showing the average expression of the top significantly enriched genes in each cluster. The top enriched genes in each cluster versus all remaining cells were calculated by the Seurat *FindAllMarkers* function with an adjusted p value <0.05, a $\log_2$ fold change >0.25, and 25% as the minimum percentage of cells expressing DEGs.
(E) Dotplot showing the percentage and average expression of the top ten genes enriched in each cluster. To avoid redundancy, histone genes ($n = 80$) enriched in cycling gene sets were excluded.
(F) UMAP plot showing the cell-cycle phase annotation according to the Seurat function *CellCycleScoring*.
(G) UMAP plot showing the combined expression of the *CXCR5* (green) and PDCD1 (red) genes.
(H) Violin plots showing the expression of the *CXCR5*, *PDCD1*, and *CXCR3* genes in each cluster.
(I) Single-cell trajectory analyzed by *monocle3* showing the interconnection (black line) among cells in different clusters based on the gene enrichment in each cluster.
(J) UMAP plot depicting cells of different clonal sizes: single, small, medium, large, and hyperexpanded.
(K) Barplot showing the number of average cells per clonotype in each cluster.
(L) Heatmap showing the percentage of overlapping clonotypes between two designated clusters in rows and columns. Only expanded clonotypes (clonal size >1) ($n = 231$) were included in the clonotype overlap analysis.
(M) Circos plots showing the overlapping clonotypes between a cluster of interest and the remaining clusters shown as connecting lines between two arcs representing the two clusters. The length of the arc represents the number of unique expanded clonotypes in a given cluster. Vertical lines against each arc show the $\log_{10}$ scaled number of cells per unique clonotype.
See also Figure S3.

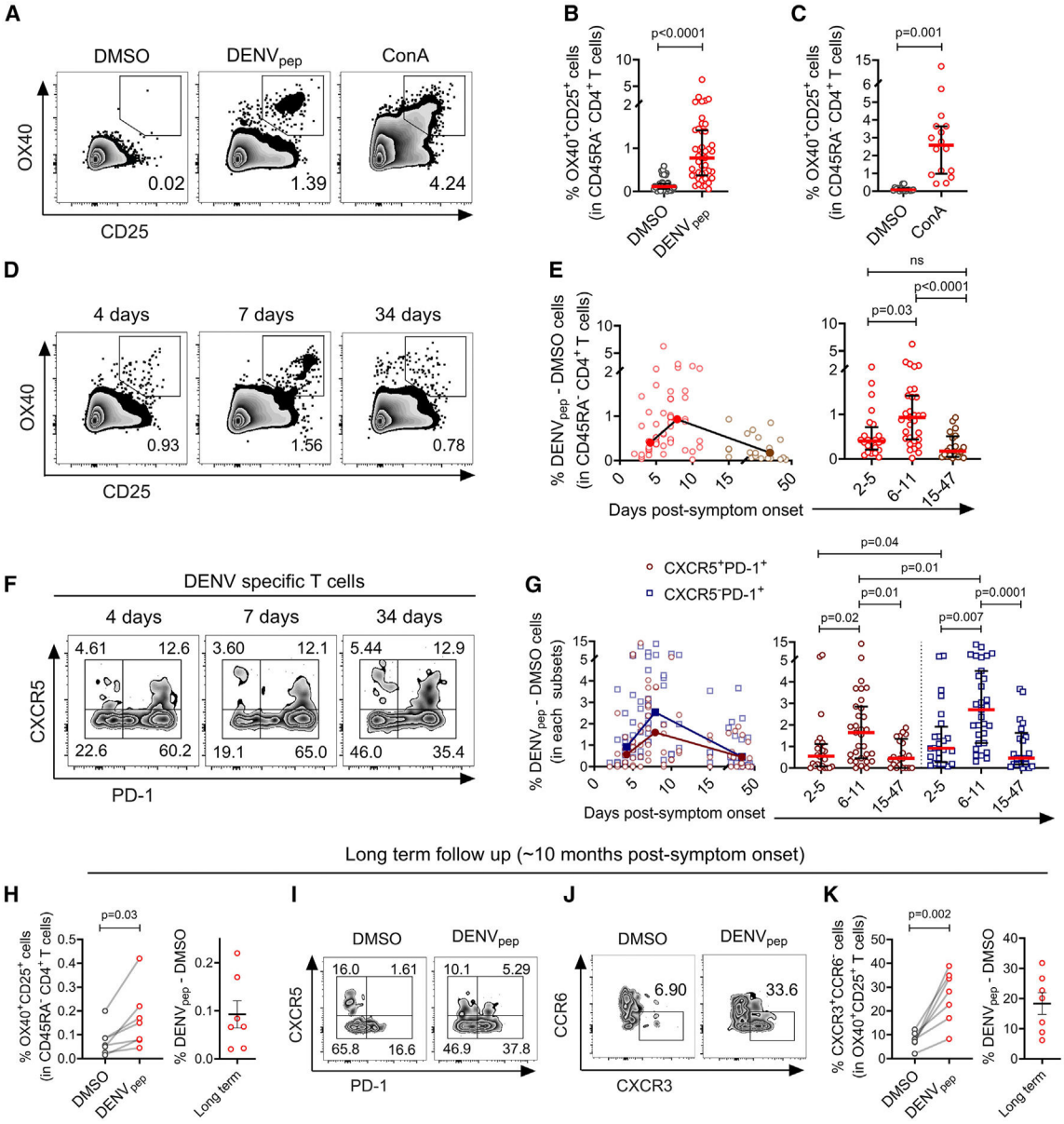

Figure 4. CXCR5^{-}PD-1^{+} cells are present in the dengue-virus-specific memory CD4^{+} T cell pool and circulate persistently in the blood of dengue-recovered individuals

(A) FACS plots showing the surface staining of OX40 (CD134) and CD25 in CD45RA^{-}CD4^{+} T cells from acute dengue in the vehicle control (DMSO), stimulation with DENV peptide megapool (DENV$_{pep}$), or concanavalin A (ConA) for 18–20 h.

(B and C) Frequency of OX40^{+}CD25^{+} T cells among CD45RA^{-}CD4^{+} T cells in acute dengue PBMCs stimulated with (B) DMSO or DENV$_{pep}$ (n = 44) or (C) DMSO or ConA (n = 16).

(D) Representative plots depicting the frequency of DENV-specific T cells among CD45RA^{-}CD4^{+} T cells in PBMC samples at 4, 7, and 34 days post symptom onset.

(E) Frequency of background (DMSO)-subtracted DENV-specific $CD45RA^{-}CD4^{+}$ T cells at continuous and grouped time points (days post symptom onset) in cross-sectional DENV samples ($n = 72$).

(F) Representative images of CXCR5 and PD-1 staining in DENV-specific $CD45RA^{-}CD4^{+}$ T cells after $DENV_{pep}$ stimulation.

(G) Percentage of T cells from the $CXCR5^{+}PD\text{-}1^{+}$ (red circles) and $CXCR5^{-}PD\text{-}1^{+}$ (blue squares) subsets from continuous and grouped time points (days post symptom onset) after subtraction from the DENV-specific background (DMSO), as shown in (E).

(H) Frequency of $OX40^{+}CD25^{+}$ memory cells among $CD45RA^{-}CD4^{+}$ T cells stimulated with DMSO or $DENV_{pep}$ in seven long-term (~10 months) follow-up individuals.

(I) Staining of CXCR5 and PD-1 in $OX40^{+}CD25^{+}$ DENV-specific memory ($CD45RA^{-}$) T cells as shown in (H).

(J and K) (J) Example FACS plots and (K) frequency of $CCR6^{-}CXCR3^{+}$ cells among $OX40^{+}CD25^{+}$ memory cells stimulated with DMSO or $DENV_{pep}$. Statistics: (B, C, H, and K) paired t test; (E and G) Kruskal-Wallis test corrected using Dunn's multiple comparisons test. ns, not significant. Data are presented as median ± IQR. See also Figure S4.

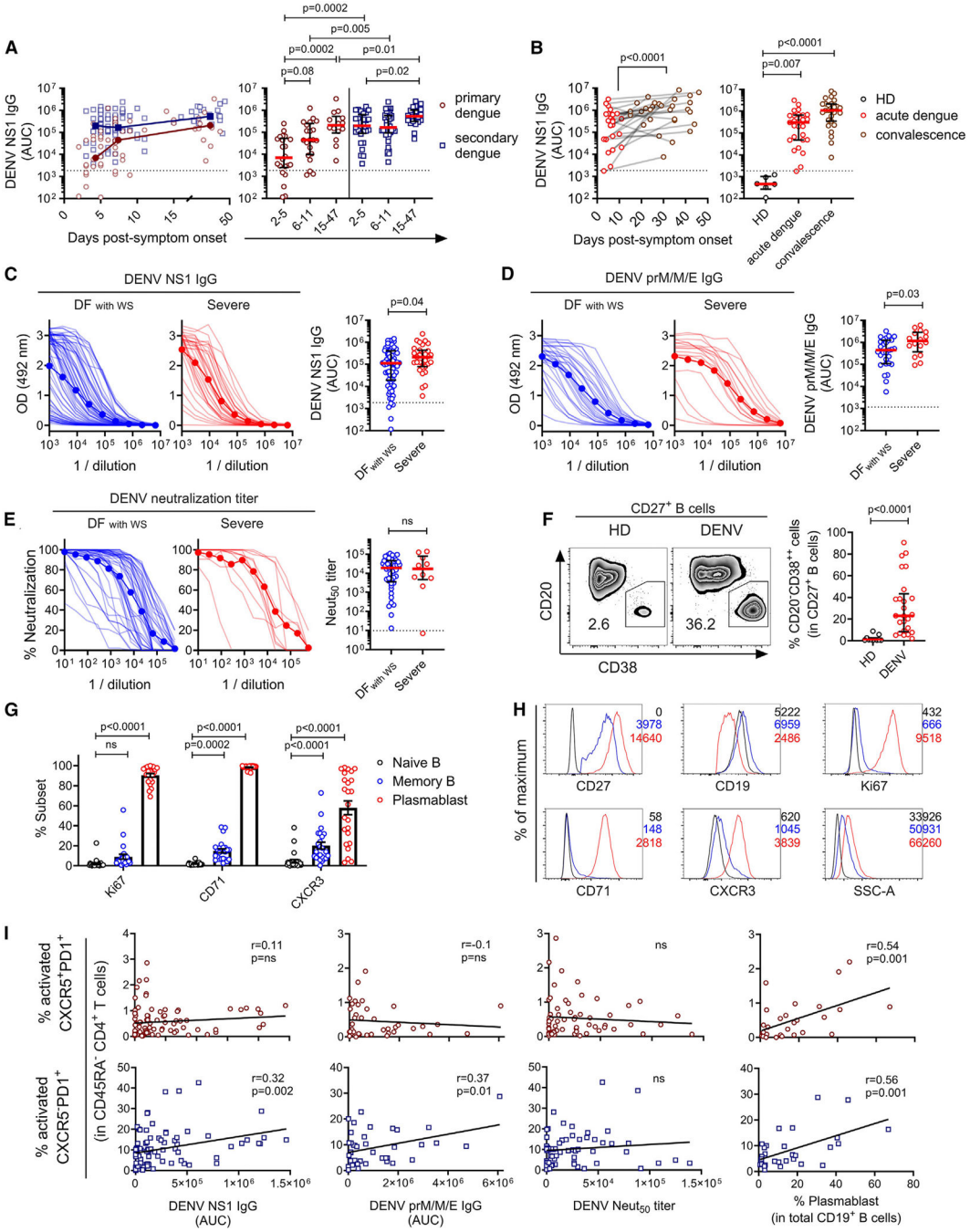

Figure 5. Activated CXCR5^{-}PD-1^{+}CD4^{+} T cells are positively associated with antibody responses and plasmablasts in dengue

(A) Scatterplots showing the quantity (area under the curve [AUC]) of anti-NS1 IgG at continuous and grouped time points (days post symptom onset) from cross-sectional cohorts of primary (n = 62) and secondary (n = 92) dengue samples.

(B) Longitudinal analysis of anti-NS1 IgG (AUC) in paired acute and convalescent dengue samples (n = 27) in comparison with DENV-seronegative HD samples.

(C) ELISA OD curves of anti-NS1 IgG in serially diluted plasma samples from DF patients with WS ($n = 70$) and severe ($n = 31$) dengue. A scatterplot was generated to compare the quantity of the anti-NS1 antibody (AUC) between the two groups.
(D) ELISA OD curves of DENV-specific structural protein (prM/M/E) IgG in DFs with WS ($n = 29$) and severe ($n = 16$) dengue samples. Scatterplot showing the levels of the anti-prM/M/E antibody (AUC) in the indicated groups.
(E) DENV-neutralizing antibody titration curves in plasma of DFs with WS ($n = 45$) and severe ($n = 10$) dengue samples. Scatterplot shows the DENV-neutralization 50 ($Neut_{50}$) titers in the indicated groups.
(F) Representative FACS plots and scatter dotplot showing the frequency of plasmablasts ($CD20^{-}CD38^{++}$) among $CD27^{+}$ B cells in HDs ($n = 11$) and DENV-infected patients (DENV) ($n = 25$).
(G) Scatter barplot showing the frequency of Ki67-, CD71-, and CXCR3-positive cells among naive and memory B cells and plasmablasts from acute dengue virus (DENV) samples. Data are shown as mean ± SEM.
(H) Histogram plots showing the geometric MFI of CD27, CD19, Ki67, CD71, CXCR3, and SSC in naive (black), memory B (blue), and plasmablast (red) cells.
(I) xy plots showing the correlations of the frequency of activated $CXCR5^{+}PD\text{-}1^{+}$ and $CXCR5^{-}PD\text{-}1^{+}$ cells with the levels of anti-NS1 ($n = 90$), anti-prM/M/E ($n = 40$) DENV-IgG, DENV-$Neut_{50}$ titer ($n = 62$), and plasmablast ($n = 30$) in acute samples.
Statistics: (A and B) Kruskal-Wallis test followed by Dunn's multiple comparisons test; (B) paired analysis by Wilcoxon signed rank test; (C–F) Mann-Whitney test; (G) two-way ANOVA with Tukey's multiple comparisons test; (I) Pearson's correlation test. ns, not significant. The dotted line in (A)–(E) represents the limit of positivity. Data are presented as median ± IQR. See also Figure S5.

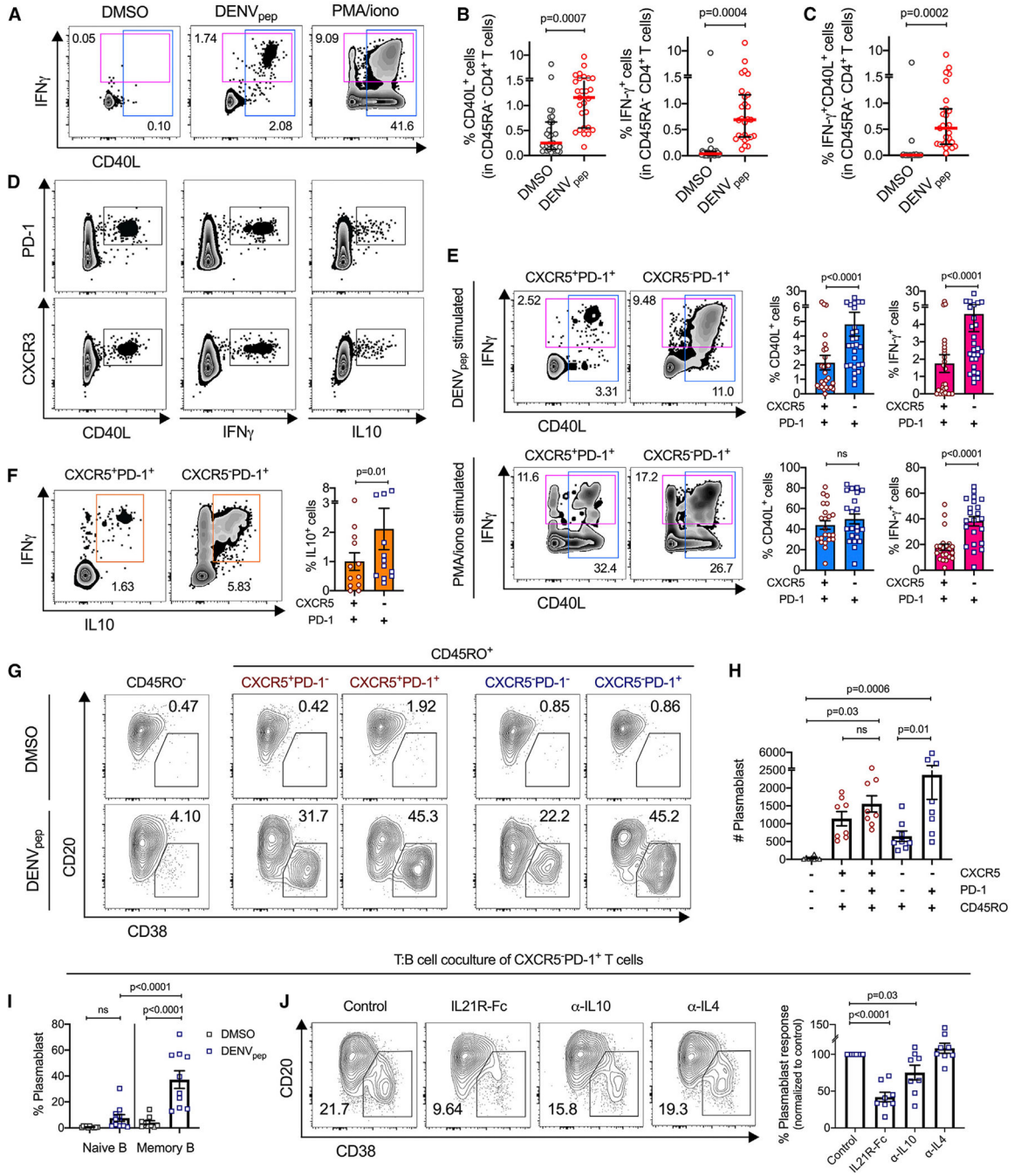

Figure 6. DENV-specific CXCR5^{-}PD-1^{+}CD4^{+} T cells are functionally potent and capable of driving plasmablast and antibody responses

(A) FACS plots showing the intracellular staining of CD40L and IFN-γ in CD45RA^{-}CD4^{+} T cells from acute dengue stimulated with DMSO, PMA/ionomycin (PMA/iono), or $DENV_{pep}$ for 6 h.

(B) Frequencies of CD40L^{+} and IFN-γ^{+} cells among CD45RA^{-}CD4^{+} T cells.

(C) Frequency of CD40L^{+}IFN-γ^{+} cells among CD45RA^{-}CD4^{+} T cells. Data are shown as median ± IQR.

(D) FACS plots showing the costaining of CD40L, IFN-γ, and IL-10 with PD-1 and CXCR3 in $CD4^+$ T cells stimulated with $DENV_{pep}$.
(E) Frequencies of $CD40L^+$ and IFN-γ^+ cells in the $CXCR5^+PD\text{-}1^+$ and $CXCR5^-PD\text{-}1^+$ subsets stimulated with $DENV_{pep}$ and PMA/iono.
(F) Plots showing the costaining of IFN-γ and IL-10 (left) and a barplot showing the frequency of $IL\text{-}10^+$ cells in the $DENV_{pep}$ condition (right).
(G) Representative FACS plots showing the frequency of plasmablasts ($CD20^-CD38^{++}$) induced in autologous cocultures of different $CD4^+$ T cell subsets and $CD20^+$ B cells from DENV-seropositive individuals cultured for 9 days in DMSO and $DENV_{pep}$ conditions.
(H) Number of plasmablasts in T:B cocultures in the presence of $DENV_{pep,}$ as shown in (G).
(I) Barplots quantifying plasmablast differentiation in cocultures of the $CXCR5^-PD\text{-}1^+$ T cell subset and naive ($CD27^-$) or memory ($CD27^+$) $CD20^+$ B cells.
(J) Example plots showing the plasmablast frequency in T:B cocultures of $CXCR5^-PD\text{-}1^+$ T cells and $CD20^+$ B cells in the presence of $DENV_{pep}$ with or without blocking conditions with IL-21R-Fc, anti-IL-10, and anti-IL-4. Right: data in the scatter barplot are background subtracted from DMSO and normalized to the control (without blocking) condition.
Statistics: (B and C) paired t test; (E and F) Wilcoxon signed-rank test; (H) one-way ANOVA with Tukey's multiple comparisons test; (I) one-way ANOVA with Bonferroni's multiple comparisons test; (J) one-way ANOVA with Dunnett's multiple comparisons test. ns, not significant. Data are presented as mean ± SEM. See also Figure S6.

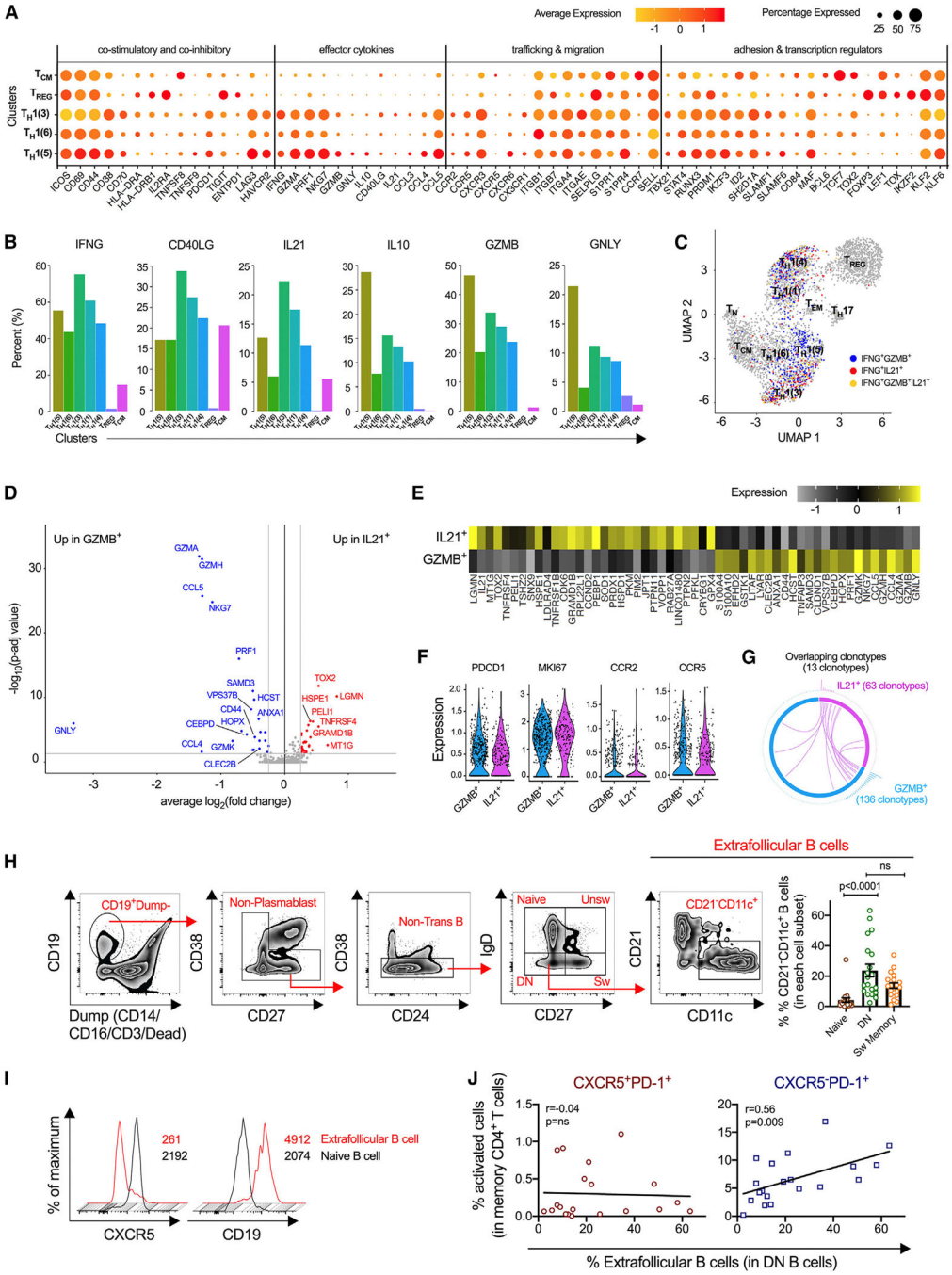

Figure 7. Distinct features and diverse clonotypes of the *helper* subset of CXCR5^{-}PD-1^{+} T cells and their strong association with the extrafollicular B cell response

(A) Dotplot showing the average expression and percentage of the indicated genes in the selected clusters.

(B) Barplots showing the percentage of cells expressing *IFNG*, *CD40LG*, *IL21*, *IL10*, *GZMB*, and *GNLY* transcripts in the indicated clusters.

(C) UMAP plot showing *IFNG*-positive cells expressing *GZMB* (*GZMB*$^{+}$), *IL21* (*IL21*$^{+}$), or both (*GZMB*$^{+}$*IL21*$^{+}$).

(D) Volcano plot showing the DEGs between the *GZMB*$^+$ and *IL21*$^+$ cell populations. Significant DEGs were calculated by Seurat *FindMarkers* function with adjusted *p* value <0.05, $\log_2$|fold change| >0.25, and 10% as minimum percentage of cells expressing DEGs.
(E) Heatmap showing the comparative average expression of all DEGs enriched in *IL21*$^+$ versus *GZMB*$^+$ cells.
(F) Violin plots showing the expression of the indicated genes in *IL21*$^+$ and *GZMB*$^+$ cells.
(G) Circos plot showing the overlapping clonotypes (connecting lines) between the *IL21*$^+$ and *GZMB*$^+$ cell populations. The length of the arc represents the number of unique clonotypes in the designated group. The vertical lines against each arc indicate the $\log_{10}$ scaled clonotype size.
(H) Representative FACS plots for phenotyping of extrafollicular (CD21$^-$CD11c$^+$) cells among double-negative (IgD$^-$CD27$^-$) CD19$^+$ B cells. The barplot shows the enrichment of the extrafollicular B cell phenotype in the indicated B cell subsets. Data are shown as mean ± SEM.
(I) Histograms depicting the comparative expression (*gMFI*) of the surface markers CXCR5 and CD19 in extrafollicular B cells (red) and naive cells (black).
(J) xy plots showing the correlations of the frequency of activated CXCR5$^+$PD-1$^+$ and CXCR5$^-$PD-1$^+$ subsets with the frequency of extrafollicular B cells in patients (n = 20) with acute dengue.
Statistics: (H) Friedman test followed by Dunn's multiple comparisons test; (J) Pearson's correlation test. ns, not significant. See also Figure S7.

KEY RESOURCES TABLE

REAGENT or RESOURCE	SOURCE	IDENTIFIER
Antibodies		
CD14, APC-eFluor 780, 61D3	eBioscience	Cat# 47-0149-42; RRID: AB_1834358
CD16, APC-eFluor 780, eBioCB16	eBioscience	Cat# 47-0168-42; RRID: AB_11220086
CD20, APC-eFluor 780, 2H7	eBioscience	Cat# 47-0209-42; RRID: AB_1272038
CD8a, APC-eFluor 780, RPA-T8	eBioscience	Cat# 47-0088-42; RRID: AB_1272046
FOXP3, PE, PCH101	eBioscience	Cat# 12-4777-42; RRID: AB_1944444
ICOS, FITC, C398.4A	eBioscience	Cat# 11-9949-82; RRID: AB_465458
Ki67, PE, SolA15	eBioscience	Cat# 12-5698-82; RRID: AB_11150954
CCR6, PE, 11A9	BD Biosciences	Cat# 559562; RRID: AB_397273
CD14, PE, MΦP9	BD Biosciences	Cat# 562691; RRID: AB_2737725
CD25, APC, M-A251	BD Biosciences	Cat# 555434; RRID: AB_398598
CD25, PE-CF594, M-A251	BD Biosciences	Cat# 562403; RRID: AB_11151919
CD38, PE/Cyanine5, HIT2	BD Biosciences	Cat# 555461; RRID: AB_395854
CD45RO, FITC, UCHL1	BD Biosciences	Cat# 555492; RRID: AB_395883
CXCR5, Alexa Fluor 647, RF8B2	BD Biosciences	Cat# 558113; RRID: AB_2737606
GZMB, PE, JES3-9D7	BD Biosciences	Cat# 561142; RRID: AB_10561690
ICOS, PE-CF594, C398.4A	BD Biosciences	Cat# 565888; RRID: AB_2869727
IFN-γ, PE-CF594, B27	BD Biosciences	Cat# 562392; RRID: AB_11153859
IL-10, Brilliant Violet 421, JES3-9D7	BD Biosciences	Cat# 564053; RRID: AB_2738566
IL-21, Alexa Fluor 647, 3A3-N2.1	BD Biosciences	Cat# 560493; RRID: AB_1645421
CCR4, TotalSeq-C0071, L291H4	BioLegend	Cat# 359425; RRID: AB_2800988
CCR6, Alexa Fluor 488, G034E3	BioLegend	Cat# 353414; RRID: AB_10916395
CCR6, PE/Cyanine7, G034E3	BioLegend	Cat# 353418; RRID: AB_10916518
CCR6, TotalSeq-C0143, G034E3	BioLegend	Cat# 353440; RRID: AB_2810563
CD11c, PE, S-HCL-3	BioLegend	Cat# 371504; RRID: AB_2616899
CD19, Brilliant Violet 785, HIB19	BioLegend	Cat# 302240; RRID: AB_2563442
CD20, PE/Cyanine7, 2H7	BioLegend	Cat# 302312; RRID: AB_314259
CD21, PE/Cyanine7, Bu32	BioLegend	Cat# 354912; RRID: AB_2561576
CD24, APC, ML5	BioLegend	Cat# 311118; RRID: AB_1877150
CD27, PE/Dazzle 594, M-T271	BioLegend	Cat# 356422; RRID: AB_2564100
CD27, TotalSeq-C0154, O323	BioLegend	Cat# 302853; RRID: AB_2800747
CD3, APC/Cyanine7, HIT3a	BioLegend	Cat# 300318; RRID: AB_314053
CD38, Brilliant Violet 421, HIT2	BioLegend	Cat# 303526; RRID: AB_10900230
CD38, Brilliant Violet 510, HIT2	BioLegend	Cat# 303540; RRID: AB_2616791
CD4, Alexa Fluor 700, RPA-T4	BioLegend	Cat# 300526; RRID: AB_493743
CD40L, PE/Cyanine7, 24-31	BioLegend	Cat# 310832; RRID: AB_2563016
CD45RA, Brilliant Violet 785, HI100	BioLegend	Cat# 304140; RRID: AB_2561369
CD71, APC, CY1G4	BioLegend	Cat# 334108; RRID: AB_10915138
CD8a, APC, RPA-T8	BioLegend	Cat# 301049; RRID: AB_2562054
CXCR3, Alexa Fluor 488, G025H7	BioLegend	Cat# 353710; RRID: AB_10962442

REAGENT or RESOURCE	SOURCE	IDENTIFIER
CXCR3, Brilliant Violet711, G025H7	BioLegend	Cat# 353732; RRID: AB_2563532
CXCR3, TotalSeq-C0140, G025H7	BioLegend	Cat# 353747; RRID: AB_2800949
CXCR5, Brilliant Violet 421, J252D4	BioLegend	Cat# 356920; RRID: AB_2562302
CXCR5, TotalSeq-C0144, J252D4	BioLegend	Cat# 356939; RRID: AB_2800968
HLA-DR, Brilliant Violet 560, L243	BioLegend	Cat# 307650; RRID: AB_2562544
IgD, FITC, IA6-2	BioLegend	Cat# 348206; RRID: AB_10613638
OX40, PE/Cyanine7, Ber-ACT35	BioLegend	Cat# 350012; RRID: AB_10901161
PD-1, Brilliant Violet 421, EH12.2H7	BioLegend	Cat# 329920; RRID: AB_10900818
PD-1, Brilliant Violet 711, EH12.2H7	BioLegend	Cat# 329928; RRID: AB_11218612
PD-1, PE, EH12.2H7	BioLegend	Cat# 329906; RRID: AB_940481
PD-1, PE/Dazzle 594, EH12.2H7	BioLegend	Cat# 329940; RRID: AB_2563658
PD-1, TotalSeq-C0088, EH12.2H7	BioLegend	Cat# 329963; RRID: AB_2800862
IL-2, Brilliant Violet 650, MQ1-17H12	BioLegend	Cat# 500334; RRID: AB_11147166
Human IL-10 antibody	R&D Systems	Cat# MAB2173-100; RRID: AB_3663041
Human IL-4 antibody	R&D Systems	Cat# MAB204-100; RRID: AB_2126745
IFN-γ mAb (1-D1K), purified	Mabtech	Cat# 3420-3-250; RRID: AB_907283
IL-21 mAb (MT21.3m), biotin	Mabtech	Cat# 3540-6-250; RRID: AB_11178374
IL-21 mAb (MT216G), purified	Mabtech	Cat# 3540-1-250; RRID: AB_3663042
Goat anti-human Ig Fab, UNLB	SouthernBiotech	Cat# 2085-01; RRID: AB_2795785
Goat Anti-Human IgG Fc, HRP	SouthernBiotech	Cat# 2014-05; RRID: AB_2795580
Goat Anti-Human IgG, HRP	SouthernBiotech	Cat# 2045-05; RRID: AB_2795676
Goat, Anti-mouse IgG, HRP	SouthernBiotech	Cat# 1030-05; RRID: AB_2619742
4G2 antibody	N/A	N/A
Hashtag 2, TotalSeq-C0252, LNH-94; 2M2	BioLegend	Cat# 394663; RRID: AB_2801032
Hashtag 3, TotalSeq-C0253, LNH-94; 2M2	BioLegend	Cat# 394665; RRID: AB_2801033
Hashtag 4, TotalSeq-C0254, LNH-94; 2M2	BioLegend	Cat# 394667; RRID: AB_2801034
Bacterial and virus strains		
DENV serotype 2 virus, strain S-16803	N/A	N/A
Biological samples		
Blood samples from hospitalized dengue patients	AIIMS Hospital, Delhi, India	N/A
Blood samples from discharged convalescent dengue patients	N/A	N/A
Healthy donor blood buffy coats	AIIMS Hospital Blood Bank, Delhi, India	N/A
Paired blood and Lymphoid tissues	AIIMS Hospital, Delhi, India	N/A
Chemicals, peptides, and recombinant proteins		
Ficoll-Paque PLUS	Cytiva Life Sciences	Cat# 17144003
RPMI 1640	Cytiva Life Sciences	Cat# SH30027
AIM-V medium (1X)	Gibco	Cat# 12055-091
DPBS (10X)	Gibco	Cat# 14200-075
Fetal Bovine Serum	Gibco	Cat# 10270-106

REAGENT or RESOURCE	SOURCE	IDENTIFIER
RPMI 1640 + Glutamax-I (1X)	Gibco	Cat# 61870-036
Pen-Strep	Gibco	Cat# 15140-122
ACK lysis buffer	Gibco	Cat# A1049201
EDTA (0.5M), pH 8.0	Invitrogen	Cat# AM9260G
Fixable Viability Dye eFluor506	Invitrogen	Cat# 65-0866-14
Fixable Viability Dye eFluor780	Invitrogen	Cat# 65-0865-14
Dnase I (1 mg/mL)	StemCell	Cat# 07900
PI/AO stain	Logos Biosystems	Cat# F23001
Concanavalin A	Sigma-Aldrich	Cat# C0412
DMSO	Sigma-Aldrich	Cat# D2650
DNase I (Roche)	Sigma-Aldrich	Cat# 11284932001
Ionomycin calcium Salt	Sigma-Aldrich	Cat# I3909
OPD tablet, 10mg	Sigma-Aldrich	Cat# P8287
Phorbol 12-myristate 13-acetate	Sigma-Aldrich	Cat# P8139
Staphylococcal enterotoxin B	Sigma-Aldrich	Cat# S4881
Trypan Blue Solution (0.4%)	Sigma-Aldrich	Cat# T8154
Tween 20	Sigma-Aldrich	Cat# P1379
Paraformaldehyde	Sigma-Aldrich	Cat# P6148
Ethanol	Merck Millipore	Cat# 100983
Hydrochloric acid, 37%	Merck Millipore	Cat# 100317
GolgiPlug Protein Transport Inhibitor (Containing Brefeldin A)	BD Biosciences	Cat# 555029
Skim milk powder	HiMedia	Cat# GRM1254
Buffer EB	Qiagen	Cat# 19086
BCP/NBT-plus for ALP	Mabtech	Cat# 3650-10
Streptavidin-ALP	Mabtech	Cat# 3310-10-1000
Human IL-21R Fc chimera, CF	R&D Systems	Cat# 991-R2-100
Dengue Virus Serotype 2 NS1 protein	Native Antigen, UK	DENV2-NS1-100
Dengue Virus Serotype 2 VLP protein	Native Antigen, UK	DENV2-VLP-100
DENV peptide megapool	Grifoni et al.[29]	N/A
Carboxymethylcellulose	Sigma-Aldrich	Cat# M0512-250
20% Paraformaldehyde aqueous solution	Electron Microscopy Sciences	Cat# 50-980-493
Bovine Serum Albumin	Sigma-Aldrich	Cat# A7030-100G
Saponin	Sigma-Aldrich	Cat# 47036-250G-F
TrueBlue Peroxidase Substrate	SeraCare	Cat# 5510-0030
Critical commercial assays		
Human IL-21 (ALP) ELISpot Kit	Mabtech	Cat# 3540-2A
Human IFN-γ/IL-10 FluoroSpot Kit	Mabtech	Cat# FSP-0107-02
Dengue IgM Capture ELISA	Abbott	Cat# 01PE20
Dengue IgG Capture ELISA	Abbott	Cat# 01PE10
Dengue NS1 Ag Microlisa	J. Mitra & Co.	Cat# IR031096

REAGENT or RESOURCE	SOURCE	IDENTIFIER
Anti-Dengue virus IgG ELISA Kit	Abcam	Cat# Ab108728
Human CXCL13/BLC/BCA-1 Quantikine ELISA Kit	R&D Systems	Cat# DCX130
Foxp3/Transcription Factor Staining Buffer Set	Invitrogen	Cat# 00-5523-00
CellTrace Violet Proliferation Kit	Invitrogen	Cat# C34557
Qubit 1X dsDNA HS Assay Kit	Invitrogen	Cat# Q32851
SPRIselect, 5mL	Beckman Coulter	Cat# B23317
HS NGS Fragment Kit (1-6000bp)	Agilent	Cat# DNF-474-0500
Capillary Storage Solution	Agilent	Cat# GP-440-0100
Chromium Next GEM Single Cell 5' Kit v2, 4 rxns	10x Genomics	Cat# 1000265
Chromium Single Cell Human TCR Amplification Kit, 16 rxns	10x Genomics	Cat# 1000252
Library Construction Kit, 16 rxns	10x Genomics	Cat# 1000190
Chromium Next GEM Chip K Single Cell Kit, 16 rxns	10x Genomics	Cat# 1000287
5' Feature Barcode Kit, 16 rxns	10x Genomics	Cat# 1000256
Dual Index Kit TN Set A, 96 rxns	10x Genomics	Cat# 1000250
Dual Index Kit TT Set A, 96 rxns	10x Genomics	Cat# 1000215
Bio-Plex Pro Human Cytokine Screening Panel, 48-plex	Bio-Rad	Cat# 12007283
Deposited data		
Single-cell RNAseq data	Gene Expression Omnibus	GSE280258
Scripts	Zenodo	https://doi.org/10.5281/zenodo.14632965
Experimental models: Cell lines		
Vero	ATCC	Cat# CCL-81; RRID: CVCL_0059
D1-4G2-4-15	ATCC	Cat# HB-112; RRID: CVCL_J890
Software and algorithms		
FlowJo V10.3.0	FlowJo, LLC	https://www.flowjo.com/
AID Elispot v7.0	AID GmbH	https://www.elispot.com/
SkanIt v6.1	Thermo Scientific	https://www.thermofisher.com/
Bio-Plex Manager v6.2	Bio-Rad	https://www.bio-rad.com/
Prism V8.4.3	GraphPad	https://www.graphpad.com/
Cell Ranger V7.0.1	10x Genomics	https://www.10xgenomics.com/
Seurat V4.3.0	Stuart et al.[28]	https://www.satijalab.org/seurat
R V4.3.1	R Core Team	https://www.r-project.org/
MAST	Finak et al.[67]	https://www.bioconductor.org/packages/release/bioc/html/MAST.html
fgsea	Korotkevich et al.[68]	https://bioconductor.org/packages/release/bioc/html/fgsea.html
Monocle3 V1.3.1	Trapnell et al.[69]	https://cole-trapnell-lab.github.io/monocle3/
scRepertoire V1.10.0	Borcherding et al.[70]	https://www.bioconductor.org/packages/release/bioc/html/scRepertoire.html
circlize	Gu et al.[71]	https://github.com/jokergoo/circlize

REAGENT or RESOURCE	SOURCE	IDENTIFIER
UpSetR	Conway et al.[72]	https://github.com/hms-dbmi/UpSetR
Other		
96 Well Round (U) Bottom Plate	Thermo Scientific	Cat# 163320
Flat-bottom Immuno 96-well MaxiSorp Plates	Thermo Scientific	Cat# 442404
Nunc MicroWell 96-well, Flat-bottom Microplate	Thermo Scientific	Cat# 136101
ep Dualfilter T.I.P.S. 2-20 μL	Eppendorf	Cat# 0030078535
ep Dualfilter T.I.P.S. 2-200 μL	Eppendorf	Cat# 0030078551
ep Dualfilter T.I.P.S. 50 - 1,000 μL	Eppendorf	Cat# 0030078578
MultiScreen IP Filter Plate	Millipore	Cat# MSIPS4510
MultiScreen IP-FL Filter Plate	Millipore	Cat# S5EJ104I07